https://doi.org/10.5194/bg-2020-358
Preprint. Discussion started: 9 October 2020

Biogeosciences Discussions
Open Access
EGU

The Seasonal Phases of an Arctic Lagoon Reveal Non-linear pH Extremes

Cale A. Miller[1,3], Christina Bonsell[2], Nathan D. McTigue[2], Amanda L. Kelley[3]

[1] Department of Evolution and Ecology, University of California Davis, Davis, CA, USA, 95616
[2] Marine Science Institute, The University of Texas at Austin, Port Aransas, TX, USA, 78373
[3] College of Fisheries and Ocean Sciences, University of Alaska Fairbanks, Fairbanks, AK, USA, 99775

Correspondence to: Cale A. Miller (cmill@ucdavis.edu; calemiller620@gmail.com)

https://doi.org/10.5194/bg-2020-358
Preprint. Discussion started: 9 October 2020

Abstract

The western Arctic Ocean, including its shelves and coastal habitats, has become a focus in ocean acidification research over the past decade as the colder waters of the region and the reduction of sea ice appear to promote the uptake of excess atmospheric CO_2. Due to seasonal sea ice coverage, high-frequency monitoring of pH or other carbonate chemistry parameters is typically limited to infrequent ship-based transects during ice-free summers. This approach has failed to capture year-round nearshore carbonate chemistry dynamics which is modulated by biological metabolism in response to abundant allochthonous organic matter to the narrow shelf of the Beaufort Sea and adjacent regions. The coastline of the Beaufort Sea comprises a series of lagoons that account for > 50 % of the land-sea interface. The lagoon ecosystems are novel features that cycle between "open" and "closed" phases (i.e., ice-free, and ice covered, respectively). In this study, we collected high-frequency pH, salinity, temperature, and PAR measurements in association with the Beaufort Lagoon Ecosystem LTER for an entire calendar year in Kaktovik Lagoon, Alaska, USA, capturing two open water phases and one closed phase. Hourly pH variability during the open water phases are some of the fastest rates reported, exceeding 0.4 units. Baseline pH varied substantially between open phase 2018 and open phase 2019 with a difference of ~ 0.2 units despite similar hourly rates of change. Salinity-pH relationships were mixed during all three phases displaying no correlation in open 2018, a negative correlation in closed 2018 – 2019, and positive correlation during open 2019. The high-frequency of pH variability could partially be explained by photosynthesis-respiration cycles as correlation coefficients between daily average pH and PAR were 0.46 and 0.64 for open 2018 and open 2019 phases, respectively. The estimated annual daily average CO_2 efflux was 5.9 ± 19.3 mmol m^{-2} d^{-1}, which is converse to the negative influx of CO_2 estimated for the coastal

https://doi.org/10.5194/bg-2020-358
Preprint. Discussion started: 9 October 2020

Beaufort Sea despite exhibiting extreme variability. Considering the geomorphic differences in Beaufort Sea lagoons, further investigation is needed to assess if there are periods of the open phase in which all lagoons are sources of carbon to the atmosphere, potentially offsetting the predicted sink capacity of the greater Beaufort Sea.

https://doi.org/10.5194/bg-2020-358
Preprint. Discussion started: 9 October 2020

1 Introduction

Acidification of the Arctic Ocean is predicted to proceed at a faster rate than lower latitude regions due to the increased solubility of CO_2 in colder waters, intrinsically lower carbonate ion concentration, and specific water mass mixing patterns (Fabry et al., 2009; Mathis et al., 2015). The acidification phenomenon which increases the dissolved inorganic carbon to alkalinity ratio reduces the natural buffering capacity of the carbonate system via a reduction in carbonate ion concentration. These processes result in low calcium carbonate saturation state and a low sea surface pH. It is estimated that the Canadian Basin, Beaufort Sea, and Chukchi Sea in the Arctic have experienced a 2.7 % shoaling of low saturation state ($\Omega < 1.25$) waters from 0 – 250 m over the past 2 decades (Qi et al., 2017; Zhang et al., 2020). Future projections anticipate a continuation of this trend with sustained, perennial, undersaturation of calcium carbonate in the Beaufort and Chukchi Seas by the year 2040, which will reduce the capacity of these waters to continually take up atmospheric CO_2 (Mathis et al., 2015). The rate at which this happens will have significant implications on the current estimates of CO_2 uptake by the coastal Chukchi and Beaufort Seas (Evans et al. 2015a). Acidification of offshore Arctic waters appear to be a consequence of increasing Pacific Winter Water intrusion due to globally warming waters and an influx of excess atmospheric CO_2 caused by the disequilibrium between air and seawater PCO_2 (Qi et al., 2017). Along the nearshore regions of the Beaufort Sea, however, coastal processes predominately drive acidification such as riverine flux of freshwater, biological metabolism, sea-ice melt from warming waters, and upwelling of the Polar Marine Layer which is an important water source for Arctic lagoons (Carstensen and Duarte, 2019; Harris et al., 2017; Miller et al., 2014; Woosley and Millero, 2020; Wynn et al., 2016).

https://doi.org/10.5194/bg-2020-358
Preprint. Discussion started: 9 October 2020

The coastal margin of the Beaufort Sea consists of biologically complex, shallow (< 6 m), discontinuous, estuarine lagoons that depict ~ 50 % of the coast from Nuvuk (Pt. Barrow) to Demarcation Bay, Alaska, USA (Dunton et al., 2006, 2012; Harris et al., 2017; Lissauer et al., 1984). The North Slope region is predominately tundra, where the annual terrestrial thaw comprises the majority of the freshwater outflow to the Beaufort Sea. Canada's Mackenzie River is the largest source of freshwater flowing into the Beaufort Sea, ~ 300 km^3 yr^{-1} (McClelland et al., 2006; Stein and Macdonald, 2004); however, many smaller rivers and streams link the terrestrial hydrography with the marine lagoon ecosystem characterized as geomorphic transition zones (Dunton et al., 2006, 2012). Barrier islands partially obstruct Beaufort Sea coastal water exchange with the lagoons, which in part are hydrographically influenced by the seasonal shifts in terrestrial freshwater flux that results in highly dynamic chemical conditions (Mouillot et al., 2007). Flow channels between the land, Arctic lagoons and the ocean are ephemeral, causing the flow of water in and out of a lagoon to be intermittent, varying on short- and long-term time scales (Dunton et al., 2012; Kraus et al., 2008). These physical flow attributes result in highly variable salinity and temperature that range from fresh to hypersaline (0 to >45), and -2 ˚C to 14 ˚C, respectively (Dunton and Schonberg, 2006; Harris et al., 2017). This variability in temperature and freshwater delivery can have a dramatic effect on carbonate chemistry thermodynamics and modify alkalinity and dissolved inorganic carbon (DIC). The seasonality of these shallow lagoons is distinguished by two principal phase states corresponding to sea ice prevalence—open and closed. The closed period during winter ice cover exhibits a non-quantifiable amount of air-sea exchange due to the physical sea ice barrier. Conversely, the open, ice-free summer period from late spring to early fall is marked by spring river discharge, air-sea exchanges, and meteorological events (McClelland et al., 2012, 2014). Episodic fluctuations in

https://doi.org/10.5194/bg-2020-358
Preprint. Discussion started: 9 October 2020

lagoon hydrography during periods of open water add to the complexity of physicochemical variability as wind-driven upwelling events coupled with tidal flux can precipitate rapid changes in these semi-isolated bodies of water (Lissauer et al., 1984).

Despite extreme variability in temperature and salinity, Arctic lagoons are home to diverse fish assemblages that include diadromous, freshwater, and marine species (Harris et al., 2017; Robards, 2014; Tibbles, 2018), many of which serve as important subsistence fisheries for Arctic communities (Craig, 1989; Griffiths et al., 1977). Arctic lagoons have relatively high diversity and abundance of benthic community invertebrates, ranging from 654 to 5,353 individuals m^{-2} with trophic linkages to birds and marine mammals (Griffiths et al., 1977, Johnson et al., 2010; Dunton et al., 2012). The benthic food web relies on both autochthonous microalgal production and allochthonous terrestrial organic matter (OM) inputs as carbon subsidies (Harris et al., 2018). The deposition of these carbon subsidies may have implications on the chemical conditions of lagoon ecosystems via enhanced remineralization during the during open and closed phases. To date, hydrographic physicochemical measurements have been mostly limited to the open [summer] season with few exceptions (Dunton and Schonberg, 2006; Kinney et al., 1971; Mathews and Stringer, 1984; Robards, 2014). To our knowledge, only a single high-frequency year-round measurement of Beaufort Sea lagoon temperature and salinity exists (Harris et al., 2017), which is insufficient for understanding how these factors including biological metabolism may impact carbonate system dynamics.

This study is the first to incorporate a high-frequency time series of salinity, temperature, PAR, and pH for an entire calendar year capturing both open and closed phases of an Arctic lagoon. The Kaktovik Lagoon located adjacent to Barter Island and the city of Kaktovik was selected for sensor package deployment. The data collected in this study were processed in part

https://doi.org/10.5194/bg-2020-358
Preprint. Discussion started: 9 October 2020

with those available from the Beaufort Lagoon Ecosystems (BLE) Long Term Ecological Research Program (LTER) and the NOAA Earth Systems Research Laboratory (ESRL). Salinity, temperature, and pH were analyzed in the time and frequency domains alongside ancillary solar radiation and water depth in order to examine potential modifiers of pH. This included estimates of carbon flux at the land-sea interface utilizing atmospheric PCO_2 measurements and comparing those with derived seawater PCO_2 estimates. The findings of this study are presented in the context of seasonal variability of oceanographic processes in an ecosystem that is part of the western coastal Arctic that is experiencing climate change.

2 Study site and methods

2.1 Kaktovik Lagoon ecosystem

Kaktovik Lagoon, Alaska (70° 6' 3" N 143° 34' 52" W), serves as one of the study sites for the National Science Foundation's Beaufort Lagoon Ecosystem (LTER). It is one of a series of coastal lagoons that fringe the Arctic National Wildlife Refuge and borders the east side of Barter Island. With a maximum depth of approximately 4.4 m, Kaktovik Lagoon has two narrow exchange pathways with adjacent water bodies (Dunton et al., 2012). One of the pathways connects to Arey Lagoon, the other links to Jago Lagoon and to the Beaufort Sea via a channel > 25 m long and < 2.5 m deep (Fig. 1). Surface freshwater inputs are limited to small tundra streams, although narrow inlets provide some exchange to adjacent Arey and Jago Lagoons, which receive terrestrial inputs from the Hulahula/Okpilak and Jago Rivers, respectively. The timing of sea ice formation varies by year but occurs between late September and October becoming landfast (fastened to the coastline) in the shallow lagoons until breakup in May or June (Dunton et al., 2006).

https://doi.org/10.5194/bg-2020-358
Preprint. Discussion started: 9 October 2020

2.2 Oceanographic sampling

A benthic mooring outfitted with a SeaBird SeaFET V2 and RBR Concerto CTD++ was deployed 8 August 2018 to 11 August 2019, with sensors roughly 10 cm from the bottom in Kaktovik Lagoon (Fig. 1). Hourly measurements of pH, salinity, and temperature (from SeaFET thermistor) were recorded (UTC) throughout the deployment period. A separate, adjacent mooring consisting of a LI-COR spherical quantum sensor in-line with a LI-1000 datalogger recorded photosynthetically active radiation (PAR µmol photons m^{-2} s^{-1}; 400-700 nm) ~30 cm from the bottom. Average PAR was integrated over three-hour time periods and recorded. In April, August, and June, the site was sampled for dissolved nutrients and physicochemical parameters within 30 cm of water surface and within 30 cm of the bottom. Physicochemical parameters were recorded with a YSI ProDSS calibrated daily before excursions. Nutrient samples were collected with a peristaltic pump fitted with Masterflex C-flex tubing, then filtered through a Geotech 0.45 µm high-capacity polyethersulfone (PES) capsule filter connected with Masterflex-C tubing and frozen at -20 ˚C until analysis. Sediment was retrieved from the seafloor by a 0.1 m^2 van Veen grab, sampled with 50 mL push core and frozen at -20 ˚C until analysis. Porewater was extracted by centrifugation of defrosted sediment, then analyzed immediately. Dissolved nutrients in water and porewater [ammonia (NH_3), nitrate + nitrite (NO_x), orthophosphate (PO_4^{3-}), and silica (SiO_2)] were measured at the Core Facilities Laboratory at The University of Texas Marine Science Institute in Port Aransas, Texas on a continuous flow-analyzer Lachat Quick Chem 8500.

2.3 Seawater chemistry and sensor calibration

https://doi.org/10.5194/bg-2020-358
Preprint. Discussion started: 9 October 2020

Discrete bottle samples were taken approximately 10 cm off the bottom proximal to the sensor on 17 August 2018 for SeaFET calibration, and 26 April 2019 for reference. Bottle samples were collected in duplicate and processed for total alkalinity-A_T and pH_T (total scale). An additional A_T sample was collected on 21 June 2019. The August 2018 sample was gathered by Van Dorn bottle, where a single sampling was used to fill duplicate bottle replicates. April 2019 duplicate samples were directly collected from depth by a peristaltic pump fitted with MasterFlex C-flex tubing. All seawater samples were placed in 500 mL borosilicate bottles and fixed with 200 µL saturated mercuric chloride and held at 4 ˚C until laboratory analysis.

A_T was measured with an open-cell titrator using 0.1 M hydrochloric acid titrant on a Metrohm Titrino 848 (Dickson et al., 2007: SOP 3b). Spectrophotometric pH_T measurements were made in duplicate using a Shimadzu 1800 outfitted with a cuvette temperature controller stabilizing temperature at 25 ˚C. The spectrophotometric pH_T was determined using *m*-cresol purple (Acros, batch # 30AXM-QN), following SOP 6b from Dickson et al. (2007). An impurity correction factor of the *m*-cresol reagent was used to adjust the final measured pH_T value (Douglas and Byrne, 2017). All salinity measurements were conducted with a YSI 3100 conductivity meter. Certified Reference Material of seawater (CRM: Batch 172, A.G., Dickson, Scripps Institute of Oceanography) was used to calculate the A_T and *m*-cresol dye uncertainty. Calibration and reference *in situ* pH_T samples were derived using the Matlab version of CO2SYS (van Heuven et al., 2011) with input parameters salinity, temperature, pH_T, and A_T using dissociation constants from Lueker et al. (2000), Dickson et al. (1990), and Uppström (1974).

A SeaFET conditioning period of 9 d was conceded from deployment on 8 August 2018 to 17 August 2018 when the calibration sample was collected. A single-point calibration was applied following previously established best practices (Bresnahan et al., 2014; Miller et al.,

https://doi.org/10.5194/bg-2020-358
Preprint. Discussion started: 9 October 2020

2018). New calibration coefficients for the SeaFET were then applied and used to calculate pH_T from the internal ISFET electrode for the entire dataset (Martz et al., 2010). The single reference sample taken on 26 April 2019 was used to compare against SeaFET measured pH_T as a check for sensor drift and robustness of calibration.

2.3.1 Uncertainty estimate

The reliability and accuracy of SeaFET sensors is dependent on estimating the total uncertainty attributable to an individual sensor's behavior and operator usage (Bresnahan et al., 2014; Gonski et al., 2018; McLaughlin et al., 2017; Miller et al., 2018; Rivest et al., 2016). A previous method for calculating the total uncertainty associated with SeaFET function has been previously proposed and was applied to this study (Miller and Kelley 2020 *in review*). Briefly, a propagated uncertainty Eq. (1) was derived by adding in quadrate the standard deviation of analytical replicates measuring CRM pH_T spectrophotometrically, a titrator uncertainty comparing measured and known A_T from CRM, the standard deviation of discrete pH_T bottle replicates, and the uncertainty associated with CO2SYS dissociation constants using the Matlab errors function described in Orr et al. (2018). An additional salinity uncertainty not described in Miller and Kelley (2020 *in review*) was added to account for the discrepancy between benchtop salinity measurements and *in situ* readings found in this study (Table S1). The final equation reads:

$$Q = \sqrt{\sigma^2_{m-cresol} + \sigma^2_{bottle\ replicates} + \sigma^2_{CO2SYS\ constants} + \sigma^2_{salinity} + AN^2_{titrator}} \quad (1)$$

where Q is the propagated uncertainty, AN is the anomaly between measured and known A_T, and σ^2 is the standard deviation of all of the uncertainty input parameters in pH units (see Miller and Kelley 2020 *in review*). From this point, the total uncertainty was calculated by taking the

https://doi.org/10.5194/bg-2020-358
Preprint. Discussion started: 9 October 2020

average of the propagated uncertainties for the calibration sample, reference sample, and bottle anomaly (Table 1). This propagated uncertainty was then applied to the entire pH_T time series.

2.4 Ancillary data acquisition

The Beaufort Lagoon Ecosystems LTER data on current velocity, water depth, and underwater PAR was accessed through the Environmental Data Initiative portal. Current velocity was used as a proxy to determine the open and closed (i.e., ice covered or ice-free) seasons for the lagoon. A velocity consistently below 2 cm s^{-1} for a period >10 h was designated as a threshold for the two phases (Fig. S1). Water depth derived from the pressure sensor was interpreted as tidal variation, where consistent frequencies in depth changes were applied for analysis (see 2.5). Instantaneous PAR measurements were used to determine daily average values for time series analysis.

2.5 Frequency Analysis

A power spectral density (PSD) analysis of pH_T, temperature, salinity, and tide was performed using the *pwelch* function in Matlab (v2020a) to determine the magnitude of variation at a given frequency during each phase: open 2018, closed 2018 – 2019, and open 2019. This function processes data as samples s^{-1}, so for 24 measurements in a day, a sampling rate of 2.78×10^{-4} was applied with a frequency of d^{-1}. A Hamming window was used for sidelobe attenuation of the analyses and the mean value for each parameter was subtracted in order to examine only the variation around the mean. Residual noise around a frequency of 0 was muted by applying a Butterworth high-pass filter with an order of 3 and cut off frequency at 1.0×10^{-5}. If two of the analyzed variables exhibit the same predominate frequency, then their variation is assumed to be

https://doi.org/10.5194/bg-2020-358
Preprint. Discussion started: 9 October 2020

correlated regardless of direction and magnitude. Previous PSD analyses with similar parameters have been shown to be considerably noisy below ~ 50 dB Hz^{-1}, thus making this value a cutoff threshold for the purposes of this study (Miller and Kelley *in review*).

2.6 A_T, PCO_2, and flux calculations

Salinity recorded by the RBR Concerto CTD++ were filtered for invalid measurements taken over the year-long time series. Measurements identified as below the freezing point of water due to the temperature-salinity relationship were removed, and a linear interpolation was performed to replace the missing values (Fig. S2). Two linear regression analyses were performed to estimate A_T, one with measured *in situ* salinity and the other with benchtop recorded values. Each analysis was constructed with the three discrete A_T samples collected on 17 August 2018, 26 April 2019, and 21 June 2019 (Table S1), where A_T is the dependent variable and salinity the independent. Benchtop values were considered to be more robust as the YSI 3100 Conductivity meter was calibrated to the manufacturer's specification, while the CTD++ was factory calibrated. For this reason, the regression from the benchtop salinity measurements were considered to be the primary hourly A_T values; however, both A_T estimates from benchtop (slope = 59.71, R2 = 0.968) and *in situ* (slope = 48.38, R2 = 0.998) salinity were used as input parameters along with measured pH_T to calculate hourly PCO_2 values using CO2SYS (see above for constants applied).

Atmospheric hourly PCO_2 averages were collected from the NOAA ESRL station at Barrow (Utqiaġvik), Alaska, USA (Thoning et al., 2020), and wind speed was acquired from automated airport weather observations from the Barter Island Airport. Using these data,

https://doi.org/10.5194/bg-2020-358
Preprint. Discussion started: 9 October 2020

a CO_2 air-sea flux for open phases 2018 and 2019 was calculated following the bulk transfer method with a gas transfer velocity constant *k* as modified by the Schmidt number (i.e., ratio of kinematic viscosity of water to gas diffusivity), which is a function of temperature and salinity. The bulk flux equation in Wanninkhof (2014) was used for the estimate:

$$F_{bulk} = 0.251 < U^2 > (Sc/660)^{-0.5}\, K_0\, (PCO_{2_w} - PCO_{2_a}) \qquad (2)$$

where *U* is wind speed in m s^{-1}, *Sc/660* is the Schimdt number calculated using the coefficients from the 4th order polynomial in Wanninkhof (2014: Table 1), K_0 is temperature and salinity dependent solubility of CO_2 in mol L^{-1} atm^{-1} calculated following the model presented in Wanninkhof (2014: Table 2), and PCO_2 is the partial pressure of CO_2 in water ($_w$) and air ($_a$) in atm. Since the Schimdt number is a function of temperature and salinity, a freshwater value was derived using the *fw* coefficients presented in (Wanninkhof, 2014). This estimate provided a more conservative flux and was, therefore, presented as the lower bound uncertainty in the estimate. The upper bound uncertainty of the flux estimate was calculated by applying the PCO_2 values into Eq. (2) derived from the salinity$_{in\ situ}$-A_T regression. These values resulted in a larger flux estimate, which is why they were set as the upper bound. Both the lower and upper bounds were then applied as the total uncertainty for the flux estimate.

2.6 Statistical applications

Relationships between pH_T and salinity were correlated by applying a quadratic fit for the closed 2018 – 2019 phase and open 2019 phase with salinity as the explanatory variable. No correlation existed for open 2018. pH_T and PAR hourly variations were collapsed by calculating the daily

https://doi.org/10.5194/bg-2020-358
Preprint. Discussion started: 9 October 2020

averages for both parameters. The average daily values for pH_T open 2018 and 2019 were then detrended to remove correlations with salinity. A Pearson's correlation coefficient was than derived between the detrended pH_T daily averages and PAR daily averages for open 2018 and open 2019.

3 Results

3.1 Time series

The year-long time series of pH_T, temperature, and salinity was recorded from 17 August 2018 to 11 Aug 2019 (Fig. 2). Based on the current velocity threshold of 2 cm s^{-1} as a proxy for sea ice cover, the 2018 open phase transitioned to a closed phase on 8 October 2018 which terminated on 22 June 2019 as the 2019 open phase began (Fig. S1). Both calibration and reference samples that were collected in duplicate have a fairly high standard deviation at 0.099 and 0.088, respectively. The large deviation between duplicate samples was the greatest source of uncertainty (see Eq. 1) for the entire pH_T time series, which shows the total uncertainty shaded in grey (Fig. 2a) and found in (Table 1). Invalid salinity values were ~ 6 % of the entire time series, with the greatest proportion of interpolated values concentrated in the closed phase (Fig.2c).

In the open phase of 2018 pH_T values were highly variable in August ranging from 7.66 to 8.40, which was the highest pH_T recorded for the entire calendar year (Fig. 3a). An upward trend in pH_T began on 21 August and steadily increased indicating a continued accuracy of the internal ISFET at low salinity. The low episodic salinity event when values were < 9 occurred from 23 August to 27 August 2018, which was after the sporadic variability in pH_T days earlier (Fig. 3). From September until freeze-up on 8 October, pH_T variability was low with the 7-d running average maintaining at ~ 8.10 and fluctuating < 0.1 units. Temperature followed a steady

https://doi.org/10.5194/bg-2020-358
Preprint. Discussion started: 9 October 2020

decrease with a negative slope of 0.12 (Fig. 3b). Salinity rose steadily although instances of large episodic events were present, and in one instance on 1 September, salinity increased from 12.9 to 23.1 in an 8 h period (Fig. 3c).

During the closed phase when Kaktovik Lagoon first became ice-covered, pH_T continued to remain somewhat invariant around ~ 8.10 as it did during the previous two open-water months (Fig. 4a). Approximately 2 weeks into the closed phase, pH_T began to steadily decrease until stabilizing in the beginning of January at ~ 7.71. pH_T varied between 7.55 and 7.85 from this point until April when another negative trend culminated at a low of 7.48. Late May saw pH_T levels increase until phase transition on 22 June 2019. Temperature stayed below -1 ˚C until late May when it began to increase concomitantly with pH_T approaching 0 ˚C (Fig. 4b). Salinity values increased from 31 at the start of ice cover reaching a maximum of 39.2 in April (Fig. 4c).

Open phase 2019 saw extreme pH_T variability beginning 21 June to 11 August 2019 with the rate of hourly change reaching as high as 0.467 units (Fig. 5a). During the first portion of this phase, the pH_T running average was consistent at ~ 8.05 and shifting only ± 0.05 units. Episodic fluctuations caused pH_T values to reach as high as 8.33. A negative trend began in late July shifting the running average to ~ 7.79, which was ~ 0.2 units lower than the running average in August 2018. Temperature increased rapidly during the first 2 weeks following break up and then remained stable around 10 ˚C (Fig. 5b). Salinity decreased steadily for the first month after break-up followed by large episodic freshening events in late July (Fig. 5c); these were similar to the events seen in the open phase of 2018.

Correlations between salinity and pH_T were inconsistent and varied by phase. Open phase 2018 pH_T was not correlated with salinity which ranged from 5 to 30, while pH_T was predominantly steady shifting only ± 0.1 units around 8.0 (Fig. 6a). The maximum range of pH_T

https://doi.org/10.5194/bg-2020-358
Preprint. Discussion started: 9 October 2020

during this period was confined to salinity values between 11.5 to 12.5. During the closed phase, pH_T correlated well with salinity, which ranged from ~ 30 to 40 (Fig. 6b). An inverse relationship between salinity and pH_T was present during this phase with an R^2 of 0.69. The opposite pattern was observed during open phase in 2019, however, where salinity and pH_T were positively correlated with an R^2 of 0.66 (Fig. 6c). The temperature relationships with salinity were due to seasonal timing rather than intrusion of water mass or mixing.

3.2 Frequency of pH variability

The PSD of pH_T during open phase 2018 and closed phase 2018 – 2019 were weak with the majority of peaks around any given frequency falling under 50 dB Hz^{-1} (Fig. 7a and b). Peaks of pH_T during open 2018 did not correspond with any regular frequencies across temperature, salinity (Fig. 7) or tide (Fig. S3), which only displayed regular peaks at a frequency of 1 and 2 d^{-1}. Consistent variability of pH_T during the closed phase was negligible but had a maximum magnitude at a frequency of 0.39 which corresponded to a peak observed with temperature (Fig. 7b and e). Open phase 2019 had a multitude of peaks with frequencies ranging from 0.5 to 7.5 d^{-1}, however most fell under 50 dB Hz^{-1} (Fig. 7c). The highest magnitude of pH_T corresponded well with tide at ~ 1 d^{-1} (Fig. 7c and S3c). Salinity also displayed a strong peak at 1 d^{-1} (Fig. 7i), sharing this frequency of variability with pH_T and tide.

3.3 pH response to PAR

Open phase 2018 and open phase 2019 daily average pH_T was compared against instantaneous underwater PAR levels recorded for both phases (Fig. 8). Open phase 2018 PAR levels were consistently lower compared to open phase 2019 as a result of the time of year the two phases

https://doi.org/10.5194/bg-2020-358
Preprint. Discussion started: 9 October 2020

were observed (Fig. 8). The detrended daily average pH_T correlated well with daily average PAR with a Pearson's correlation coefficient of 0.469 (*p-value* = 0.005). In early August 2018, PAR levels > 5 µmol photons m^{-2} s^{-1} were not representative of, high, daily average pH_T. This was a deviation from the general trend of the open 2018 phase in which daily average pH_T was positively correlated with instantaneous PAR (Fig. 8a). In late August and September, high values of daily average pH_T > 8.20 coincided with spikes in instantaneous PAR that exceeded 10 µmol photons m-^{2} s^{-1} (Fig. 8a).

Open phase 2019 daily average pH_T was overall more variable than open phase 2018 with values from 7.66 in early August to 8.09 in late June (Fig.8b). The detrended daily average pH_T had a more robust correlation with daily average underwater PAR than in 2018 with a Pearson's correlation of 0.643 (*p-value* < 0.000). The highest PAR values were recorded in mid-July; however, this did not correlate with the highest daily average pH_T which was observed in late June. Consistent high values of PAR in mid-July corresponded to relatively flat daily average pH_T (Fig. 8b). A reduction in instantaneous PAR to values below 15 µmol photons m^{-2} s^{-1} in late July was linked with a gradual decrease in daily average pH_T. During this 11-d period, daily average pH_T dropped from 8.06 to 7.71, and only began to increase again when instantaneous PAR exceeded 25 µmol photons m^{-2} s^{-1} for consecutive days.

3.4 Flux Estimation

Carbon flux estimates for open phase 2018 and open phase 2019 showed dramatically different results with 13 instances exceeding a flux > 10 µmol CO_2 m^{-2} min^{-1} compared to 302 instances in open phase 2019 (Fig. 9)—where 10 µmol CO_2 m^{-2} min^{-1} is ≈ to 2 mmol CO_2 m^{-2} d^{-1} which is the equivalent magnitude, but opposite of the estimated annual mean sea-air flux for the coastal

https://doi.org/10.5194/bg-2020-358
Preprint. Discussion started: 9 October 2020

Beaufort Sea, -2 mmol CO_2 m^{-2} d^{-1} (Evans et al, 2015a). The episodic events of flux from the atmosphere into seawater was greater in 2018 with 21 instances < -10 μmol CO_2 m^{-2} min^{-1} compared to a single instance in 2019. The maximum lower bound uncertainty for open phase 2018 was estimated at 2.23 μmol CO_2 m^{-2} min^{-1} whereas the upper bound was 10.67 μmol CO_2 m^{-2} min^{-1} (Fig. 9a). Overall, wind speed correlated poorly with CO_2 flux in 2018 (R^2 = 0.13). The highest frequency of robust wind speeds occurred in October but resulted in only a minor atmospheric flux into seawater as the majority of values were between 2 and -5 μmol CO_2 m^{-2} min^{-1} (Fig. 9a).

Open phase 2019 had an estimated CO_2 flux as high as 105 μmol CO_2 m^{-2} min^{-1}, which occurred in early August (Fig. 9b). Over a 5.6 d period in late July, CO_2 flux was > 10 μmol CO_2 m^{-2} min^{-1} for more than 90 % of the time reaching a high of 78 μmol CO_2 m^{-2} min^{-1}. The maximum lower bound uncertainty estimate for open phase 2019 was 5.5 μmol CO_2 m^{-2} min^{-1} with an upper bound uncertainty of 8.56 μmol CO_2 m^{-2} min^{-1}. Wind speed was found to be significantly correlated with CO_2 flux (*p-value* < 0.0001, R^2 = 0.53) in 2019 and, thus, cogently different from open phase 2018.

4 Discussion

Kaktovik Lagoon was an ideal location for a year-long deployment to capture the three phases (i.e., open 2018, closed 2018 – 2019, and open 2019) of environmental conditions in the coastal Arctic. The study site displayed annual pH variability in the context of a unique lagoon where geographical and physical features of this site represent a semi-closed system with narrow passages to the sea and only small tundra stream inputs. The stochastic events of pH captured in this system are some of the most dramatic hourly pH rates of change recorded to date (Cyronak

https://doi.org/10.5194/bg-2020-358
Preprint. Discussion started: 9 October 2020

et al., 2020; Hofmann et al.; 2011; Kapsenberg et al., 2015; Kapsenberg and Hofmann, 2016; Takeshita et al., 2015). These findings represent a system that is often in tenuous equilibrium resulting in dramatic fluctuations of CO_2 outgassing and differing magnitudes of pH sensitivity to temperature and salinity. The extreme nature of these habitats displays the resilience of the micro and macro faunal community that undoubtedly modify seawater pH via biological processes. While this study was able to capture physical and chemical conditions of the lagoon, future work should be directed toward understanding how community organization in the lagoon ecosystem affect pH variability.

4.1 Kaktovik Lagoon and pH-salinity relationship

A crucial finding from this year-long time series was the disparity between the pH_T-salinity relationship during the open 2018, closed 2018 – 2019, and open 2019 phases. Sequentially through the time series, the pH_T-salinity relationship was non-existent, negatively correlated, and positively correlated, indicating that multiple processes drive pH variability at differing magnitudes at a seasonal-phase resolution. Given the myriad processes such as temperature-salinity relationships with carbonate chemistry, current- and wind-driven flux between the sediment-water interface and the air-sea interface, as well as photosynthesis and respiration cycles (Carstensen and Duarte, 2019; Hagens et al., 2014; Rassmann et al., 2020; Zeebe and Wolf-Gladrow, 2001), it is unsurprising that salinity was observed as only a moderate and intermittent driver of pH_T variability in Kaktovik Lagoon. This is despite the multitude of salinity changes that shift in time due to the discharge from rivers and tundra streams, seasonal ice-formation and break up, and water column stratification, all which would be expected to fluctuate pH predictably. The features intrinsic to Kaktovik Lagoon are likely important factors

https://doi.org/10.5194/bg-2020-358
Preprint. Discussion started: 9 October 2020

responsible for the degree of pH_T-salinity interdependence and provide a lens that elucidates pH_T altering processes that are less germane to physical oceanographic open-ocean mechanisms such as temperature and salinity.

The characteristics of the Beaufort Sea lagoon ecosystems are unique features of the coastline and exist as an interface between terrestrial inputs and seawater with each lagoon varying in its connectivity to the Beaufort and freshwater sources. These lagoons temporarily trap large amounts of allochthonous particulate organic carbon—which is expected to increase with warming temperatures—and sediment as river and stream discharge are temporarily mismatched between spring freshet and ice-covered margins (Dunton et al., 2006; Schreiner et al., 2013). The lagoons adjacent to Kaktovik (Arey and Jago) are likely to be more exogenously influenced due to greater connectivity to the Beaufort Sea, and the Okpilak, Hulahula, and Jago Rivers. Thus, the modification of pH_T within Kaktovik Lagoon provides a baseline that is likely dissimilar to adjacent lagoons providing an in-depth examination of the internal processes of a "closed system" such as biological metabolism and sediment flux that can drive seasonal pH variability and explain the annual shifts in moderate salinity dependence.

In the open phase of 2018, pH_T values were observed to be > 8.05 despite the striking range of salinity from 5 to 30. This included an event that modulated salinity from 13 to 23 over an 8 h period, which was correlated with high NW winds at ~ 20 m s^{-1}. This suggests that higher salinity waters from the adjacent Arey Lagoon connecting the Beaufort Sea may have mixed into the bottom waters were the pH sensor was located. The stability of salinity toward the new higher values indicates the validity of this data. Further, the salinity range in open phase 2018 tested the limits of the ISFET senor which had not been tested for stability below a salinity of 9 (Gonski et al., 2018), but appeared stable here. Open phase 2019 had a narrower range of salinity

https://doi.org/10.5194/bg-2020-358
Preprint. Discussion started: 9 October 2020

which correlated robustly with pH_T as values above 8.0 were only observed when salinity was > 25. While the interdependence between pH_T and salinity can be variable in nearshore systems (Carstensen and Duarte, 2019), the degree to which pH_T remained stable across a range of salinity in open 2018 is notable. Similarly, a recent study in Stefansson Sound (~ 160 km west of Kaktovik Lagoon) found that salinity-dependent nearshore pH_T varied by year, however, the range of salinity was more attenuated than in Kaktovik (Muth et al. 2020 *in review*). The disparity between the salinity-pH_T correlation between the open 2018 and open 2019 phases was observable in the frequency response of variability. In open phase 2018, the PSD of pH_T was low and mostly incongruent with the frequency response of salinity. This was not the case in open phase 2019 where the highest PSD was recorded at the same frequency (1.03 d^{-1}) as salinity, which was slightly offset from the PSD peak in tidal frequency at 0.98 d^{-1}. These associations suggest that events driving low salinity such as stream runoff were likely too irregular, or too low of flux, relative to the weak but consistent tidal signal driving open ocean exchange. This also corresponds to the lower range of salinity observed in open phase 2019 than in open phase 2018.

4.2 High-frequency pH in Arctic and Subarctic

Interannual variability of pH_T between open phase 2018 and open phase 2019 is not dependent on a single driving factor, including time of season. In the 2018 open phase pH_T was consistently high during a period when daylength was shortening and temperatures were falling. The increasing trend of consistently high pH_T continued into the closed phase. Conversely, August 2019 pH_T had a running average that was ~ 0.2 units lower than 2018 and continued a downward trend until the end of the time series. Similar findings have shown significantly different

https://doi.org/10.5194/bg-2020-358
Preprint. Discussion started: 9 October 2020

interannual variability in pH along the Arctic coast that exceeded the running average difference of ~ 0.2 observed in Kaktovik Lagoon by double (Muth et al. *in review)*. This seasonally shifting dependence of pH_T on salinity has implications for carbonate chemistry dynamics and how pH_T is modified. Freshwater input from rivers have been shown to increase dissolved inorganic carbon and lower A_T which can decouple the linear relationships between calcium carbonate saturation state, PCO_2, and pH (Cai, 2011; Hales et al., 2016; Salisbury et al., 2008). Glacial ice-melt in subarctic waters, however, is unique in that its profile is low in PCO_2 and A_T (Evans et al., 2014). Both modes of freshwater carbonate chemistry decoupling may be present in Kaktovik, but evidence here suggests that salinity is a non-reliable indicator of these decoupling mechanisms as pH_T values can exist across a wide range of salinity and even lack relationship during open phases.

Open phase 2019 displayed highly variable pH_T relative to open phase 2018 with an inconsistent frequency of variability. In the subarctic waters off Alaska's south-central coast, Jakolof Bay had a consistent seasonal trend in pH_T variability with hourly rates of change as high as 0.18 (Miller and Kelley 2020, *in review*). While these rates of hourly change are considered high (Hofmann et al., 2011), both open phases in Kaktovik were more than double that (0.401 and 0.467) of Jakolof Bay. These extreme rates of change in Kaktovik can be partially explained by the photosynthetic and respiratory activity within the lagoon.

4.3 PAR and pH

This study found robust correlations between underwater PAR and daily average pH_T. The episodic nature of pH_T variability in Kaktovik Lagoon was more prevalent during periods of high underwater PAR indicative of coupled diurnal photosynthesis-respiration cycles. Consistent

https://doi.org/10.5194/bg-2020-358
Preprint. Discussion started: 9 October 2020

levels of PAR appeared to be associated with sustained daily average pH_T while drops in PAR lowered the overall baseline pH_T. The rapid response of baseline pH_T to PAR highlights the tenuous balance between the biological processes that drive pH_T modification. This phenomenon is counter to what was observed in the subarctic macroalgal-dominated waters of Jakolof Bay where the system maintained net autotrophy for a period > 60 days (Miller and Kelley, *in review*). Possible explanations for the precarity of a dominant autotrophic or heterotrophic system may be due to the shallow nature of the lagoon and frequent homogeneity of the water column. In the shallow waters of the lagoon, high winds easily resuspend organic material, enhance respiration, and increase light attenuation (Capuzzo et al., 2015; Moriarty et al., 2018). Thus, small decreases in underwater PAR can lead to net heterotrophy. This supports the sediment "food bank" hypothesis as continuous primary production is not needed to sustain heterotrophic activity, since stored, labile, benthic OM can accumulate in shallow environments fueling respiration (Harris et al., 2018; Mincks et al., 2005). A "bank" of OM could explain why high levels of PAR led to a sustained pH_T, and any instantaneous drop in PAR was immediately followed a decrease in daily average pH_T. This would suggest that high levels of PAR are only able to offset high rates of heterotrophy which are sustained by the seasonal accumulation of carbon subsidies from autochthonous ice algae, phytoplankton, and influx of OM from terrestrial sources—which are likely to vary annual.

4.4 Sea ice effects on carbonate chemistry

A unique feature of ice covered Arctic coastal waters is the negative relationship between pH_T and salinity, which was observed here and in previous studies (Fransson et al., 2013; Miller et al., 2011; Muth et al., *in review*; Nomura et al., 2006). In the open ocean, salinity is positively

https://doi.org/10.5194/bg-2020-358
Preprint. Discussion started: 9 October 2020

correlated with A_T as higher salinity increases the difference between conservative cations to anions. Furthermore, A_T positively correlates with pH, and a higher A_T is associated with a higher buffering capacity. The formation of sea ice, however, induces cryoconcentration of DIC via active rejection of HCO_3^- during freezing and exclusion of other ions creating high salinity brine drainage (Fransson et al., 2013; Hare et al., 2013; Miller et al., 2011). The immediate effect of high DIC concentration can lead to the precipitation of $CaCO_3$ in the form of ikaite (a polymorph of $CaCO_3 \cdot 6H_2O$) along the bottom of bulk ice formation generating CO_2 as a product of the reaction and leading to a decrease in pH (Fransson et al., 2013; Hare et al., 2013; Rysgaard et al., 2012). In addition, the extreme salinity and temperature in winter affect carbonate chemistry by modulating solubility, where an increase in salinity decreases CO_2 solubility, and colder temperatures increase CO_2 solubility. These salinity and temperature conditions result in a volatile thermodynamic stability of CO_2 where salinity effects outweigh temperature effects and can facilitate a degassing of CO_2 (Papadimitriou et al., 2004).

The continually decreasing pH_T observed in this study suggests that these carbon concentrating corollaries of sea ice formation may be in effect and contribute to the negative relationship observed between pH_T and salinity. That is, if there is no outgassing of CO_2, the relative increase in DIC and concomitant decrease in pH will be equal to that of salinity. During ice coverage, the running average of pH_T decreased from 7.93 in the beginning of November, to 7.56 in late April, and mirrors the under-ice salinity trend. This decrease is nearly identical to the 0.4 pH drop observed in the upper 2 m below the ice in Amundson Gulf from the November to April period (Fransson et al., 2013). While this phenomenon could explain the general decreasing trend between pH_T and salinity, it would be remiss to state that this negative correlation is entirely driven by cryoconcentration and ikaite formation. What is more likely is

https://doi.org/10.5194/bg-2020-358
Preprint. Discussion started: 9 October 2020

that cryocentration is occurring in tangent with accumulated aerobic respiration byproducts overtime, and the high frequency of pH_T variability is the result of biological and thermodynamic processes on carbonate chemistry.

4.5 Under ice variability in pH

The frequency of pH_T variability under ice cover was inconsistent. The PSD was weak overall during the closed phase but had a peak at 0.39 d^{-1}, which corresponded to a peak in temperature around the same frequency 0.36 d^{-1}. The temperature range of 1.9 ˚C during the closed phase can affect carbonate chemistry thermodynamics potential modulating pH by ~ 0.036; however, this is less than the derived pH_T uncertainty. The other factor driving pH_T variability is biological respiration. Data sonde measurements of dissolved oxygen recorded in late April showed bottom waters reaching lows of 5.0 mg L^{-1} (43 % saturation) compared to surface levels of 11.5 mg L^{-1} (94 % saturation) (Table S1). The stratification of oxygen in this case can likely be associated with burgeoning PAR levels in April. Previous studies have shown increases in pH are associated with photosynthesis during ice-cover, which is more prevalent proximal to bulk ice resulting in higher pH at the surface compared to the bottom (Matson et al., 2014). Other factors driving pH variability could be due to the competition between anaerobic and aerobic metabolism in low oxygenated water, and the transfer of reduced metabolites from bioirrigation (Aller, 1982, 2001; Zakem et al., 2020). Efflux of reduced metabolites from the sediment can lead to high concentrations of reduced inorganic nitrogen if oxygen concentrations are low and oxidation processes slow (Aller, 2001; Middelburg and Levin, 2009). Discrete samples taken in April found high concentrations of reduced nitrogen in the bottom waters (Table S1). If oxygen levels begin to increase in late spring due to photosynthesis, the subsequent oxidation of nitrogen

https://doi.org/10.5194/bg-2020-358
Preprint. Discussion started: 9 October 2020

and other accumulated reduced metabolites could decrease pH as was seen from mid-April to mid-May. Due to limited under-ice sampling, however, there is no way to determine the trajectory of oxygen decrease or exact timing of under ice photosynthesis. The only other mechanism potentially supplying oxygen to the lagoon would be associated with water mass exchange via tide. According to the frequency analysis, there is limited evidence showing a correlated frequency peak between pH_T and tide, indicating that tidal exchange may be restricted or not a modulator of pH_T during the closed phase. Without measuring dissolved oxygen, however, it remains unclear if oxygen is the determinant factor driving pH_T modification during the closed phase.

4.6 Arctic lagoons as carbon source to atmosphere

The estimates of CO_2 flux during the open phases of 2018 and 2019 were an *a posteriori* method to examine the drivers of pH variability in Kaktovik Lagoon. Following this approach, comparisons between pH_T rate of change and estimated CO_2 flux did not correlate, suggesting that outgassing rates were not significant enough to raise *in situ* pH. Rather, the analysis showed that the estimated lagoon CO_2 flux varied substantially by year and appears at times to be a source of CO_2 to the atmosphere. This is counter to other studies that measured carbon flux at a lagoon in the far western Beaufort (Elson Lagoon), where this site was categorized as a carbon sink; however, these lagoons differ in size, residence time, and connectivity to adjacent water bodies (Lougheed et al., 2020). Overall, the western Arctic Ocean is thought to be a carbon sink (Evans et al., 2015a; Laruelle et al., 2014); although Mathis et al. (2012) described occasional storm-induced upwelling events across the Beaufort Sea shelf that cause CO_2 efflux to the atmosphere. In this study, the variability in estimated flux from the lagoon appeared to be a

https://doi.org/10.5194/bg-2020-358
Preprint. Discussion started: 9 October 2020

function of baseline pH_T more than wind driven stress. Open phase 2018 had a higher baseline pH_T (8.01 – 8.18) than open phase 2019 (8.04 – 7.72), and despite wind speeds comparable to open phase 2019, resulted in less estimated CO_2 efflux to the atmosphere. Conversely, open phase 2019 maintained a lower baseline pH_T which promoted favorable disequilibrium (i.e., difference between PCO_{2sw} and PCO_{2a}) conditions that only needed wind stress as a catalyst. Since flux preceded low pH_T values, and outgassing did not decrease hourly pH_T, the mechanisms driving low pH and PCO_2—likely biological respiration— transcend the counterbalance of outgassing.

The flux estimates in this study suggest that the novel characteristics of coastal lagoons should be considered anomalous compared to the greater across shelf Arctic coast, defined as waters north of 70 ˚N and 100 ˚W (Bakker et al., 2014). The current classification of the coastal Arctic does not account for lagoons as specific ecosystems. Thus, the western Arctic coastal ocean is defined as a relatively homogenous area 1.2 x 10^{12} m^2 along the Chukchi and Beaufort Seas extending 400 km offshore (Evans et al., 2015a). The coastal Beaufort Sea under this definition is estimated to have an annual mean carbon uptake of 8.5 Tg C yr^{-1} without ice, and a daily annual mean flux of -2.1 mmol CO_2 m^{-2} d^{-1} (Evans et al., 2015a). Recent evidence, however, has shown that previous estimates of the carbon sink capacity of the Arctic Ocean have been overestimated, suggesting that current and increasing riverine discharge will cause a reduction in A_T ultimately decreasing its potential to absorb CO_2 (Woosley and Millero, 2020). While the lagoon ecosystems comprise a small proportion of the greater Beaufort Sea shelf, they encompass > 50 % of its coastline with significant freshwater inputs that can lower the carbon sink capacity (Dunton et al., 2006; Woosley and Millero, 2020). It is suggested here that certain lagoons, including Kaktovik, are likely episodic sources of CO_2 to the atmosphere during open

https://doi.org/10.5194/bg-2020-358
Preprint. Discussion started: 9 October 2020

phases. The daily average (± s.d.) CO_2 flux for Kaktovik Lagoon during open phase 2018 and 2019 was -2.2 ± 6.5 and 14.6 ± 23.9 mmol CO_2 m^{-2} d^{-1}, respectively. Over the entire calendar year that encompasses both open phases during which sensors were deployed, the annual daily average flux was 5.9 ± 19.3 mmol CO_2 m^{-2} d^{-1} for the entire calendar year. If integrated over the entire open phase (51.58 d in 2018 and 49.38 d in 2019), and the area of Kaktovik Lagoon, estimates suggest a net carbon flux of -2.68 x 10^{-5} Tg C $open_{18}^{-1}$ in open 2018 and 1.67 x 10^{-4} Tg C $open_{19}^{-1}$ in open 2019. It is noted that these estimates are for incomplete open phases as the data presented here do not comprise the entirety of each seasons due the scheduling of SeaFET deployment and recovery. If incorporating all the lagoons along the coast, it is plausible that the source of CO_2 from the lagoon ecosystems would partially offset the carbon sink capacity previously established, particularly when considering that the estimated daily annual average flux is at times substantially greater (5.9 ± 19.3 mmol CO_2 m^{-2} d^{-1}), and opposite, of current estimates (-2.1 mmol CO_2 m^{-2} d^{-1}) (Evans et al., 2015a; Mathis et al., 2015). Further studies that can capture high-frequency carbonate chemistry variability are needed though to determine the degree and frequency of the Beaufort lagoon ecosystems' air-sea carbon exchange.

There is a fair amount of confidence in these estimates because the A_T-salinity correlation was robust (R^2 = 0.968) and the regression coefficients were proximal to other A_T-salinity regressions for the Gulf of Alaska and the western coastal Arctic, despite being derived from only three discrete samples (Evans et al., 2015b; Shadwick et al., 2011; Yamamoto-Kawai et al., 2005). Further, the overall uncertainty of the flux estimates was low. The main source of deviation was associated with higher PCO_2 values calculated from the A_T-salinity$_{in\ situ}$ regression. This made up the upper bound of uncertainty, thus, the conclusions drawn here are from the more conservative flux estimates. The effect of fresh water on the gas transfer velocity

https://doi.org/10.5194/bg-2020-358
Preprint. Discussion started: 9 October 2020

comprised the lower bound of the uncertainty and was negligible overall. For the flux estimates presented here, a homogenous water column with respect to pH was assumed, given that discrete sonde measurements only showed pH stratification during the ice-covered season (Table S1). This is not to suggest that salinity and temperature driven stratification do not exist, rather that the evidence here suggests pH_T water column homogeneity. For example, pH_T during open phase 2018 did not correlate with salinity as values > 8.01 were present across a salinity range of 25. In cases where pH_T positively correlated with salinity as seen during open phase 2019, a freshwater stratification would suggest that low salinity at the surface would be associated with lower pH_T, and likely increase CO_2 flux as there would be a greater disequilibrium between the lagoon and the air. According to the quadratic fit between pH_T and salinity, lower pH_T at the surface associated with freshwater stratification would outweigh the A_T estimates based on salinity by an order of magnitude if there was a salinity difference of 10 between the surface and bottom waters. Thus, freshwater stratification at the surface would likely exceed our upper bound flux uncertainty and increase efflux rates. Further, any modulation of flux by temperature on the gas transfer velocity are less than the estimated upper bound uncertainty and considered negligible.

5 Conclusions

This study presents the first high-frequency pH time series for the open and under ice phases in the coastal Arctic lagoon system. Uncertainty estimates for pH_T were higher than desired but describe general trends and relative rates of change that are informative for understanding pH variability. The extremely low anomaly between the reference pH_T sample and the SeaFET suggest that the uncertainty is likely lower than estimated. pH can vary dramatically by year for the open phases and is likely a function of PAR availability and the amount of OM delivered

https://doi.org/10.5194/bg-2020-358
Preprint. Discussion started: 9 October 2020

from terrestrial sources as the balance between system autotrophy and heterotrophy were tenuous. This resulted in hourly pH_T rates of change > 0.4 units. Under ice pH variability exhibited complexities, and we postulate that multiple drivers of pH variability such as carbonate chemistry thermodynamics, ikaite precipitation, and sediment efflux were all contributing mechanisms. It is apparent that further studies of carbonate chemistry dynamics at the sediment-water interface are needed to help elucidate porewater effects on bottom water pH variability during the ice cover phase, as well as continuous oxygen measurements. Estimated CO_2 outgassing during the open phase was not a significant factor driving pH_T variability due to the collinearity of wind stress and the infrequent convergence between disequilibrium and wind speed. However, carbon flux estimates suggest that the Beaufort lagoon ecosystems may be a substantial source of carbon to the atmosphere, which is counter to previous studies predicting coastal Arctic waters as a CO_2 sink. These results highlight the need for further investigation of the Beaufort lagoon ecosystems in the context of carbonate chemistry dynamics, as these processes can affect the diverse biological communities that are present here, and aid in understanding western coastal Arctic biogeochemical dynamics.

Data availability: All data accessed from the Beaufort Lagoon Ecosystems LTER is available on the Environmental Data initiative. See reference section for access links.

Author Contributions: Cale A. Miller, NM, CB, and ALK conceptualized the manuscript thesis. CAM performed the data analysis and data visualization. ALK performed initial data QA/QC for pH data. ALK, NM, and CB performed lab analyses. Cale A. Miller performed all data analysis. CAM wrote the original manuscript draft with minor contributions in the

introduction from ALK and CB in the methods. ALK, CB, and NM reviewed and edited the manuscript.

Competing interests: The authors declare no conflict of interest.

Acknowledgments: We thank R/V Proteus captains Ted Dunton and John Dunton for expert mooring deployment and recovery. We additionally thank K. Dunton, S. Jump, J. Kasper for logistical and field assistance. This work took place in the traditional and current homeland of the Kaktovikmuit.

Financial support: This material is based upon work supported by the National Science Foundation under award #1656026

References

Aller, R.: Carbonate Dissolution in Nearshore Terrigenous Muds - the Role of Physical and Biological Reworking, J. Geol., 90(1), 79–95, 1982.

Aller, R.C.: Transport and reactions in the bioirrigated zone, in: The Benthic Boundary Layer: Transport Processes and Biogeochemistry, edited by: Boudreau, B. P. and Jorgensen, B. B., pp. 269–301, Oxford University Press., 2001.

Bakker, D. C. E., Pfeil, B., Smith, K., Hankin, S., Olsen, A., Alin, S. R., Cosca, C., Harasawa, S., Kozyr, A., Nojiri, Y., O'Brien, K. M., Schuster, U., Telszewski, M., Tilbrook, B., Wada, C., Akl, J., Barbero, L., Bates, N. R., Boutin, J., Bozec, Y., Cai, W.-J., Castle, R. D., Chavez, F. P., Chen, L., Chierici, M., Currie, K., de Baar, H. J. W., Evans, W., Feely, R. A., Fransson, A., Gao, Z., Hales, B., Hardman-Mountford, N. J., Hoppema, M., Huang, W.-J., Hunt, C. W., Huss, B., Ichikawa, T., Johannessen, T., Jones, E. M., Jones, S. D., Jutterström, S., Kitidis, V., Körtzinger, A., Landschützer, P., Lauvset, S. K., Lefèvre, N., Manke, A. B., Mathis, J. T., Merlivat, L.,

Metzl, N., Murata, A., Newberger, T., Omar, A. M., Ono, T., Park, G.-H., Paterson, K., Pierrot, D., Ríos, A. F., Sabine, C. L., Saito, S., Salisbury, J., Sarma, V. V. S. S., Schlitzer, R., Sieger, R., Skjelvan, I., Steinhoff, T., Sullivan, K. F., Sun, H., Sutton, A. J., Suzuki, T., Sweeney, C., Takahashi, T., Tjiputra, J., Tsurushima, N., van Heuven, S. M. a. C., Vandemark, D., Vlahos, P., Wallace, D. W. R., Wanninkhof, R. and Watson, A. J.: An update to the Surface Ocean CO_2 Atlas (SOCAT version 2), Earth Syst. Sci. Data, 6(1), 69–90, doi:https://doi.org/10.5194/essd-6-69-2014, 2014.

Beaufort Lagoon Ecosystems LTER and J. Kasper. 2020. Circulation dynamics: currents, waves, temperature measurements from moorings in lagoon sites along the Alaska Beaufort Sea coast, 2018-ongoing ver 2. Environmental Data Initiative. https://doi.org/10.6073/pasta/3475cdbb160a9f844aa5ede627c5f6fe

Beaufort Lagoon Ecosystems LTER, Core Program. 2020. Photosynthetically active radiation (PAR) time series from lagoon sites along the Alaska Beaufort Sea coast, 2018-ongoing ver 1. Environmental Data Initiative. https://doi.org/10.6073/pasta/ced2cedd430d430d9149b9d7f1919729

Beaufort Lagoon Ecosystems LTER, Core Program. 2020. physicochemical water column parameters and hydrographic time series from river, lagoon, and open ocean sites along the Alaska Beaufort Sea coast, 2018-ongoing ver 1. Environmental Data Initiative. https://doi.org/10.6073/pasta/e0e71c2d59bf7b08928061f546be6a9a

Beaufort Lagoon Ecosystems LTER, Core Program. 2020. Time series of water column pH from lagoon sites along the Alaska Beaufort Sea coast, 2018-ongoing ver 1. Environmental Data Initiative. https://doi.org/10.6073/pasta/9305328d0f1ed28fbb2d7cf56c686786

Bresnahan, P. J., Martz, T. R., Takeshita, Y., Johnson, K. S. and LaShomb, M.: Best practices for autonomous measurement of seawater pH with the Honeywell Durafet, Methods Oceanogr., 9, 44–60, doi:10.1016/j.mio.2014.08.003, 2014.

Cai, W.-J.: Estuarine and Coastal Ocean Carbon Paradox: CO2 Sinks or Sites of Terrestrial Carbon Incineration?, in Annual Review of Marine Science, Vol 3, vol. 3, edited by C. A. Carlson and S. J. Giovannoni, pp. 123–145, Annual Reviews, Palo Alto., 2011.

Capuzzo, E., Stephens, D., Silva, T., Barry, J. and Forster, R. M.: Decrease in water clarity of the southern and central North Sea during the 20th century, Glob. Change Biol., 21(6), 2206–2214, doi:10.1111/gcb.12854, 2015.

Carstensen, J. and Duarte, C. M.: Drivers of pH Variability in Coastal Ecosystems, Environ. Sci. Technol., 53(8), 4020–4029, doi:10.1021/acs.est.8b03655, 2019.

Craig, P. C.: Subsistence fisheries at coastal villages in the Alaskan Arctic, 1970–1986. Biological Papers of the University of Alaska, 24, 131-152, 1989.

Cyronak, T., Takeshita, Y., Courtney, T. A., DeCarlo, E. H., Eyre, B. D., Kline, D. I., Martz, T., Page, H., Price, N. N., Smith, J., Stoltenberg, L., Tresguerres, M. and Andersson, A. J.: Diel

temperature and pH variability scale with depth across diverse coral reef habitats, Limnol. Oceanogr. Lett., 5(2), 193–203, doi:10.1002/lol2.10129, 2020.

Dickson, A.: Thermodynamics of the Dissociation of Boric-Acid in Potassium-Chloride Solutions from 273.15-K to 318.15-K, J. Chem. Eng. Data, 35(3), 253–257, doi:10.1021/je00061a009, 1990.

Dickson A. G., Sabine C. L. & Christian J. R.: Guide to best practices for ocean CO_2 measurements, in: PICES Special Publication, edited by: Dickson, A. G., Sabine, C. L., and Christian, J. R., 2007.

Douglas, N. K. and Byrne, R. H.: Achieving accurate spectrophotometric pH measurements using unpurified meta-cresol purple, Mar. Chem., 190, 66–72, doi:10.1016/j.marchem.2017.02.004, 2017.

Dunton, K.H., and S.V. Schonberg.: Barter Island to Demarcation Bay: A preliminary benthic survey of Arctic coastal lagoons. Fairbanks: Final Report to USF&WS, Arctic Refuge, 2006.

Dunton, K. H., Weingartner, T. and Carmack, E. C.: The nearshore western Beaufort Sea ecosystem: Circulation and importance of terrestrial carbon in arctic coastal food webs, Prog. Oceanogr., 71(2), 362–378, doi:10.1016/j.pocean.2006.09.011, 2006.

Dunton, K. H., Schonberg, S. V. and Cooper, L. W.: Food Web Structure of the Alaskan Nearshore Shelf and Estuarine Lagoons of the Beaufort Sea, Estuaries Coasts, 35(2), 416–435, doi:10.1007/s12237-012-9475-1, 2012.

Evans, W., Mathis, J. T. and Cross, J. N.: Calcium carbonate corrosivity in an Alaskan inland sea, Biogeosciences, 11(2), 365–379, doi:10.5194/bg-11-365-2014, 2014.

Evans, W., Mathis, J. T., Cross, J. N., Bates, N. R., Frey, K. E., Else, B. G. T., Papkyriakou, T. N., DeGrandpre, M. D., Islam, F., Cai, W.-J., Chen, B., Yamamoto-Kawai, M., Carmack, E., Williams, W. J. and Takahashi, T.: Sea-air CO_2 exchange in the western Arctic coastal ocean, Glob. Biogeochem. Cy., 29(8), 1190–1209, doi:10.1002/2015GB005153, 2015a.

Evans W., Mathis, J. T., Ramsey, J. and Hetrick J.: On the frontline: Tracking ocean acidification in an Alaskan shellfish hatchery, PloS One, 10(7), e0130384, doi:10.1371/journal.pone.0130384, 2015b.

Fabry, V., McClintock, J., Mathis, J. and Grebmeier, J.: Ocean Acidification at High Latitudes: The Bellwether, Oceanogr., 22(4), 160–171, doi:10.5670/oceanog.2009.105, 2009.

Fransson, A., Chierici, M., Miller, L. A., Carnat, G., Shadwick, E., Thomas, H., Pineault, S. and Papakyriakou, T. N.: Impact of sea-ice processes on the carbonate system and ocean acidification at the ice-water interface of the Amundsen Gulf, Arctic Ocean, J. Geophys. Res. Oceans, 118(12), 7001–7023, doi:10.1002/2013JC009164, 2013.

https://doi.org/10.5194/bg-2020-358
Preprint. Discussion started: 9 October 2020

Gonski, S. F., Cai, W.-J., Ullman, W. J., Joesoef, A., Main, C. R., Pettay, D. T. and Martz, T. R.: Assessment of the suitability of Durafet-based sensors for pH measurement in dynamic estuarine environments, Estuar. Coast. Shelf Sci., 200, 152–168, doi:10.1016/j.ecss.2017.10.020, 2018.

Griffiths, W.B., J.K. Den Beste, and P.C.: Fisheries investigations in a coastal lagoon region of the Beaufort Sea (Kaktovik Lagoon, Alaska). Arctic Gas Biol. Report Ser. 40(2): 1–190, 1977.

Hagens, M., Hunter, K. A., Liss, P. S. and Middelburg, J. J.: Biogeochemical context impacts seawater pH changes resulting from atmospheric sulfur and nitrogen deposition, Geophys. Res. Lett., 41(3), 935–941, doi:10.1002/2013GL058796, 2014.

Hales, B., Suhrbier, A., Waldbusser, G. G., Feely, R. A. and Newton, J. A.: The Carbonate Chemistry of the "Fattening Line," Willapa Bay, 2011–2014, Estuar. Coast., 1–14, doi:10.1007/s12237-016-0136-7, 2016.

Hare, A. A., Wang, F., Barber, D., Geilfus, N.-X., Galley, R. J. and Rysgaard, S.: pH evolution in sea ice grown at an outdoor experimental facility, Mar. Chem., 154, 46–54, doi:10.1016/j.marchem.2013.04.007, 2013.

Harris, C. M., McClelland, J. W., Connelly, T. L., Crump, B. C. and Dunton, K. H.: Salinity and Temperature Regimes in Eastern Alaskan Beaufort Sea Lagoons in Relation to Source Water Contributions, Estuar. Coast., 40(1), 50–62, doi:10.1007/s12237-016-0123-z, 2017.

Harris, C. M., McTigue, N. D., McClelland, J. W. and Dunton, K. H.: Do high Arctic coastal food webs rely on a terrestrial carbon subsidy?, Food Webs, 15, e00081, doi:10.1016/j.fooweb.2018.e00081, 2018.

Hofmann, G. E., Smith, J. E., Johnson, K. S., Send, U., Levin, L. A., Micheli, F., Paytan, A., Price, N. N., Peterson, B., Takeshita, Y., Matson, P. G., Crook, E. D., Kroeker, K. J., Gambi, M. C., Rivest, E. B., Frieder, C. A., Yu, P. C. and Martz, T. R.: High-Frequency Dynamics of Ocean pH: A Multi-Ecosystem Comparison, Plos One, 6(12), e28983, doi:10.1371/journal.pone.0028983, 2011.

Johnson, S. W., Thedinga, J. F., Neff, A. D., & Hoffman, C. A.: Fish fauna in nearshore waters of a barrier island in the western Beaufort Sea, Alaska, 2010.

Kapsenberg, L. and Hofmann, G. E.: Ocean pH time-series and drivers of variability along the northern Channel Islands, California, USA, Limnol. Oceanogr., 61(3), 953–968, doi:10.2307/26628461, 2016.

Kapsenberg, L., Kelley, A. L., Shaw, E. C., Martz, T. R. and Hofmann, G. E.: Near-shore Antarctic pH variability has implications for the design of ocean acidification experiments, Sci. Rep., 5, srep09638, doi:10.1038/srep09638, 2015.

Kinney, P., Schell, D., Dygas, J., Nenahlo, R. and Hall, G.: Nearshore Currents, in: Baseline data study of the Alaskan Arctic aquatic environment, Kinney, P., Schell, D., Alexander, V., Burrell, D., Cooney, R. and Naidu, A. S., Univ. Alaska, Inst. Mar. Sci. Rep. R-72-3, 1971.

https://doi.org/10.5194/bg-2020-358
Preprint. Discussion started: 9 October 2020

Kraus, N. C., Patsch, K. and Munger, S.: Barrier Beach Breaching from the Lagoon Side, With Reference to Northern California, U.S. Army Engineer Research and Development Center, Coast and Hydraulics Laboratory, 2008.

Laruelle, G. G., Lauerwald, R., Pfeil, B. and Regnier, P.: Regionalized global budget of the CO_2 exchange at the air-water interface in continental shelf seas, Glob. Biogeochem. Cy., 28(11), 1199–1214, doi:10.1002/2014GB004832, 2014.

Lissauer, I. M., Hachmeister, L. E., Morson, B. J.: Atlas of the Beaufort Sea, U.S. Dep. of Trans., U.S. Coast Guard, Office of Res. and Dev., 1984.

Lougheed, V. L., Tweedie, C. E., Andresen, C. G., Armendariz, A.M., Escarzaga, S. M. and Tarin, G.: Patterns and drivers of carbon dioxide concentration sin aquatic ecosystems of the Arctic coastal tundra, Glob. Biogeochem. Cy., 34(3), e2020GB006552, doi:10.1029/2020GB006552, 2020.

Lueker, T. J., Dickson, A. G. and Keeling, C. D.: Ocean pCO_2 calculated from dissolved inorganic carbon, alkalinity, and equations for K_1 and K_2: Validation based on laboratory measurements of CO_2 in gas and seawater at equilibrium, Mar. Chem., 70(1), 105–119, doi:10.1016/S0304-4203(00)00022-0, 2000.

Macdonald, R.W., E. Sakshaug, and R. Stein.: The Arctic Ocean: modern status and recent climate change, in: The organic carbon cycle in the Arctic Ocean, edited by: R. Stein and R.W. Macdonald, pp. 6–21, Berlin: Springer, 2004.

Martz, T. R., Connery, J. G. and Johnson, K. S.: Testing the Honeywell Durafet® for seawater pH applications, Limnol. Oceanogr. Methods, 8(5), 172–184, doi:10.4319/lom.2010.8.172, 2010.

Mathis, J. T., Pickart, R. S., Byrne, R. H., McNeil, C. L., Moore, G. W. K., Juranek, L. W., Liu, X., Ma, J., Easley, R. A., Elliot, M. M., Cross, J. N., Reisdorph, S. C., Bahr, F., Morison, J., Lichendorf, T. and Feely, R. A.: Storm-induced upwelling of high pCO_2 waters onto the continental shelf of the western Arctic Ocean and implications for carbonate mineral saturation states, Geophys. Res. Lett., 39(7), L07606, doi:10.1029/2012GL051574, 2012.

Mathis, J. T., Cross, J. N., Evans, W. and Doney, S. C.: Ocean Acidification in the Surface Waters of the Pacific-Arctic Boundary Regions, Oceanogr., 28(2), 122–135, doi:10.5670/oceanog.2015.36, 2015.

Matson, P. G., Washburn, L., Martz, T. R. and Hofmann, G. E.: Abiotic versus Biotic Drivers of Ocean pH Variation under Fast Sea Ice in McMurdo Sound, Antarctica, PloS One, 9(9), e107239, doi:10.1371/journal.pone.0107239, 2014.

Matthews, J. B. and Stringer, W. J.: Spring breakup and flushing of an Arctic lagoon estuary, J. Geophys. Res. Oceans, 89(C2), 2073–2079, doi:10.1029/JC089iC02p02073, 1984.

McClelland, J. W., Déry, S. J., Peterson, B. J., Holmes, R. M. and Wood, E. F.: A pan-arctic evaluation of changes in river discharge during the latter half of the 20th century, Geophys. Res. Lett., 33(6), doi:10.1029/2006GL025753, 2006.

McClelland, J. W., Holmes, R. M., Dunton, K. H. and Macdonald, R. W.: The Arctic Ocean Estuary, Estuar. Coast., 35(2), 353–368, doi:10.1007/s12237-010-9357-3, 2012.

McClelland, J. W., Townsend-Small, A., Holmes, R. M., Pan, F., Stieglitz, M., Khosh, M. and Peterson, B. J.: River export of nutrients and organic matter from the North Slope of Alaska to the Beaufort Sea, Water Resor. Res., 50(2), 1823–1839, doi:10.1002/2013WR014722, 2014.

McLaughlin, K., Dickson, A., Weisberg, S. B., Coale, K., Elrod, V., Hunter, C., Johnson, K. S., Kram, S., Kudela, R., Martz, T., Negrey, K., Passow, U., Shaughnessy, F., Smith, J. E., Tadesse, D., Washburn, L. and Weis, K. R.: An evaluation of ISFET sensors for coastal pH monitoring applications, Reg. Stud. Mar. Sci., 12, 11–18, doi:10.1016/j.rsma.2017.02.008, 2017.

Middelburg, J. J. and Levin, L. A.: Coastal hypoxia and sediment biogeochemistry, Biogeosciences, 6(7), 1273–1293, doi:https://doi.org/10.5194/bg-6-1273-2009, 2009.

Miller, C. A., Pocock, K., Evans, W. and Kelley, A. L.: An evaluation of the performance of Sea-Bird Scientific's SeaFET^{TM} autonomous pH sensor: considerations for the broader oceanographic community, Ocean Sci., 14(4), 751–768, doi:https://doi.org/10.5194/os-14-751-2018, 2018.

Miller, L. A., Carnat, G., Else, B. G. T., Sutherland, N. and Papakyriakou, T. N.: Carbonate system evolution at the Arctic Ocean surface during autumn freeze-up, J. Geophys. Res. Oceans, 116(C9), doi:10.1029/2011JC007143, 2011.

Miller, L. A., Macdonald, R. W., McLaughlin, F., Mucci, A., Yamamoto-Kawai, M., Giesbrecht, K. E. and Williams, W. J.: Changes in the marine carbonate system of the western Arctic: patterns in a rescued data set, Polar Res., 33(1), 20577, doi:10.3402/polar.v33.20577, 2014.

Mincks, S. L., Smith, C. R. and DeMaster, D. J.: Persistence of labile organic matter and microbial biomass in Antarctic shelf sediments: evidence of a sediment 'food bank,' Marine Ecol. Prog. Ser., 300, 3–19, 2005.

Moriarty, J. M., Harris, C. K., Friedrichs, M. A. M., Fennel, K. and Xu, K.: Impact of Seabed Resuspension on Oxygen and Nitrogen Dynamics in the Northern Gulf of Mexico: A Numerical Modeling Study, J. Geophys. Res. Oceans, 123(10), 7237–7263, doi:10.1029/2018JC013950, 2018.

Mouillot, D., Dumay, O. and Tomasini, J. A.: Limiting similarity, niche filtering and functional diversity in coastal lagoon fish communities, Estuar. Coast. Shelf Sci., 71(3), 443–456, doi:10.1016/j.ecss.2006.08.022, 2007.

Nomura, D., Yoshikawa-Inoue, H. and Toyota, T.: The effect of sea-ice growth on air–sea CO_2 flux in a tank experiment, Tellus B Chem. Phys. Meteorol., 58(5), 418–426, doi:10.1111/j.1600-0889.2006.00204.x, 2006.

Orr, J. C., Epitalon, J.-M., Dickson, A. G. and Gattuso, J.-P.: Routine uncertainty propagation for the marine carbon dioxide system, Mar. Chem., 207, 84–107, doi:10.1016/j.marchem.2018.10.006, 2018.

Papadimitriou, S., Kennedy, H., Kattner, G., Dieckmann, G. S. and Thomas, D. N.: Experimental evidence for carbonate precipitation and CO_2 degassing during sea ice formation, Geochim. Cosmochim. Acta, 68(8), 1749–1761, doi:10.1016/j.gca.2003.07.004, 2004.

Qi, D., Chen, L., Chen, B., Gao, Z., Zhong, W., Feely, R. A., Anderson, L. G., Sun, H., Chen, J., Chen, M., Zhan, L., Zhang, Y. and Cai, W.-J.: Increase in acidifying water in the western Arctic Ocean, Nat. Clim. Change, 7(3), 195–199, doi:10.1038/nclimate3228, 2017.

Rassmann, J., Eitel, E. M., Lansard, B., Cathalot, C., Brandily, C., Taillefert, M. and Rabouille, C.: Benthic alkalinity and dissolved inorganic carbon fluxes in the Rhône River prodelta generated by decoupled aerobic and anaerobic processes, Biogeosciences, 17(1), 13–33, doi:https://doi.org/10.5194/bg-17-13-2020, 2020.

Rivest, E. B., O'Brien, M., Kapsenberg, L., Gotschalk, C. C., Blanchette, C. A., Hoshijima, U. and Hofmann, G. E.: Beyond the benchtop and the benthos: Dataset management planning and design for time series of ocean carbonate chemistry associated with Durafet®-based pH sensors, Ecol. Inform., Complete(36), 209–220, doi:10.1016/j.ecoinf.2016.08.005, 2016.

Robards, M. D.: Coastal lagoon community and ecological monitoring in the Southern Chukchi Sea National Park Unit over five decades- Status and 2012 field sampling report. National Park Service, Fairbanks, AK, 2014.

Rysgaard, S., Glud, R. N., Lennert, K., Cooper, M., Halden, N., Leakey, R. J. G., Hawthorne, F.C. and Barber, D.: Ikaite crystals in melting sea ice - implications for pCO_2 and pH levels in Arctic surface waters, The Cryos., 6, 901–908, doi:10.5194/tc-6-901-2012, 2012.

Salisbury, J. E., Vandemark, D., Hunt, C. W., Campbell, J. W., McGillis, W. R. and McDowell, W. H.: Seasonal observations of surface waters in two Gulf of Maine estuary-plume systems: Relationships between watershed attributes, optical measurements and surface pCO_2, Estuar. Coast. Shelf Sci., 77(2), 245–252, doi:10.1016/j.ecss.2007.09.033, 2008.

Schreiner, K. M., Bianchi, T. S., Eglinton, T. I., Allison, M. A. and Hanna, A. J. M.: Sources of terrigenous inputs to surface sediments of the Colville River Delta and Simpson's Lagoon, Beaufort Sea, Alaska, J. Geophys. Res. Biogeosciences, 118(2), 808–824, doi:10.1002/jgrg.20065, 2013.

Shadwick, E. H., Thomas, H., Chierici, M., Else, B., Fransson, A., Michael, C., Miller, L. A., Mucci, A., Niemi, A., Papakyriakou, T. N. and Tremblay, J.-E.: Seasonal variability of the inorganic carbon system in the Amundsen Gulf region of the southeastern Beaufort Sea, Limnol. Oceanogr., 56(1), 303–322, doi:10.4319/lo.2011.56.1.0303, 2011.

Stein, R. and Macdonald, R. W.: Organic carbon budget: Arctic Ocean vs. Global Ocean in: The organic carbon cycle in the Arctic Ocean, edited by: R. Stein and R.W. Macdonald, pp. 315–322, Berlin: Springer, 2004.

https://doi.org/10.5194/bg-2020-358
Preprint. Discussion started: 9 October 2020

Takeshita, Y., Frieder, C. A., Martz, T. R., Ballard, J. R., Feely, R. A., Kram, S., Nam, S., Navarro, M. O., Price, N. N. and Smith, J. E.: Including high-frequency variability in coastal ocean acidification projections, Biogeosciences, 12(19), 5853–5870, doi:https://doi.org/10.5194/bg-12-5853-2015, 2015.

Thoning, K. W., Crotwell, A. M. and J. W. Mund, Atmospheric Carbon Dioxide Dry Air Mole Fractions from continuous measurements at Mauna Loa, Hawaii, Barrow, Alaska, American Samoa, and South Pole. 1973-2019, Version 2020-08 Notional Oceanic and Atmospheric Administration (NOAA), Global Monitoring Laboratory (GML), Boulder, Colorado, USA http://doi.org/10.151138/yaf1-bk21 FTP pat: ftp://aftp.cmdl.noaa.gov/data/greenhouse_gases/co2/in-situ/surface/

Tibbles, M.: The seasonal dynamics of coastal Arctic lagoons in Northwest Alaska, M.Sc. thesis, December. College of Fisheries and Ocean Sciences, University of Alaska Fairbanks, 2018.

Uppström, L. R.: The boron/chlorinity ratio of deep-sea water from the Pacific Ocean, Deep Sea Res. Oceanogr. Abstr., 21, 161–162, doi:10.1016/0011-7471(74)90074-6, 1974.

van Heuven, S., Pierrot, D., Rae, J. W. B., Lewis, E., and Wallace, D.W. R.: MATLAB Program Developed for CO_2 System Calculations Department of Energy, Oak Ridge, Tennessee, 2011.

Wanninkhof, R.: Relationship between wind speed and gas exchange over the ocean revisited, Limnol. Oceanogr. Methods, 12(6), 351–362, doi:10.4319/lom.2014.12.351, 2014.

Woosley, R. J. and Millero, F. J.: Freshening of the western Arctic negates anthropogenic carbon uptake potential, Limnol. Oceanogr., 65(8), 1834–1846, doi:10.1002/lno.11421, 2020.

Wynn, J. G., Robbins, L. L. and Anderson, L. G.: Processes of multibathyal aragonite undersaturation in the Arctic Ocean, J. Geophys. Res. Oceans, 121(11), 8248–8267, doi:10.1002/2016JC011696, 2016.

Yamamoto-Kawai, M., Tanaka, N. and Pivovarov, S.: Freshwater and brine behaviors in the Arctic Ocean deduced from historical data of δO^{18} and alkalinity (1922–2022 A.D.), J. Geophys. Res. Oceans, 110(C10), doi:10.1029/2004JC002793, 2005.

Zakem, E. J., Mahadevan, A., Lauderdale, J. M. and Follows, M. J.: Stable aerobic and anaerobic coexistence in anoxic marine zones, ISME J., 14(1), 288–301, doi:10.1038/s41396-019-0523-8, 2020.

Zeebe, R. E. and Wolf-Gladrow, D. A.: CO_2 in seawater equilibrium, kinetics, isotopes, Elsevier, Amsterdam; New York., 2001.

Zhang, Y., Yamamoto-Kawai, M. and Williams, W. J.: Two Decades of Ocean Acidification in the Surface Waters of the Beaufort Gyre, Arctic Ocean: Effects of Sea Ice Melt and Retreat From 1997–2016, Geophys. Res. Lett., 47(3), e60119, doi:10.1029/2019GL086421, 2020.

https://doi.org/10.5194/bg-2020-358
Preprint. Discussion started: 9 October 2020

Table 1. Calibration and reference bottle data for SeaFET. Propagated uncertainty, for each bottle, and the calculated total pH uncertainty value as overall average (in bold).

Date & Time	*Source*	*pH_T internal electrode*	*Propagated uncertainty*	*Anomaly: | bottle sample - SeaFET |*
17 Aug. 2018	SeaFET	8.076	—	
	Bottle sample	8.073*	0.1600	—
26 Apr. 2018	SeaFET	7.576	—	
	Bottle sample	7.582	0.1006	0.0061
Total uncertainty				**0.0889**

https://doi.org/10.5194/bg-2020-358
Preprint. Discussion started: 9 October 2020

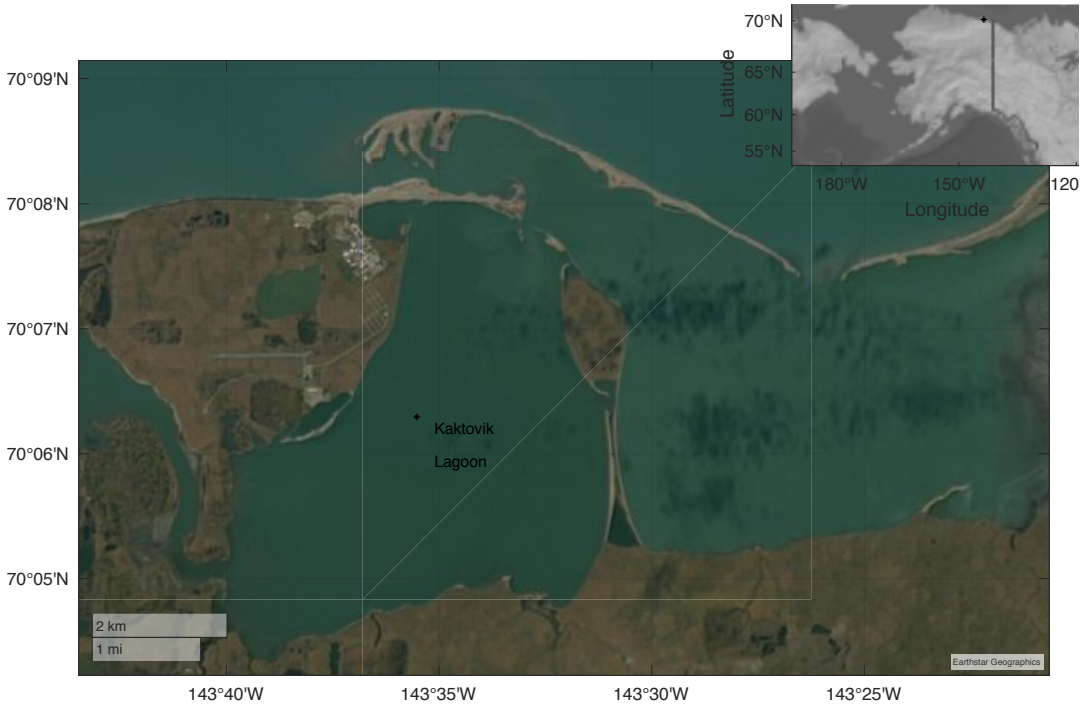

Figure 1. Study site at Kaktovik Lagoon along the Beaufort Sea Coastline.

https://doi.org/10.5194/bg-2020-358
Preprint. Discussion started: 9 October 2020

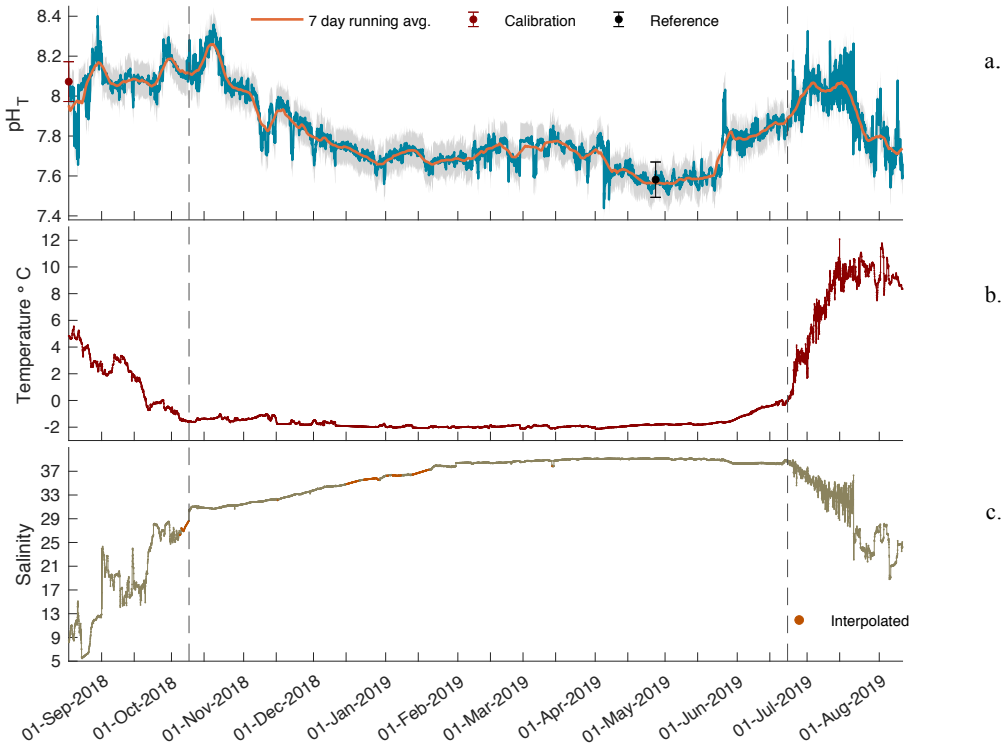

Figure 2. Times series of pH$_T$ (a), temperature (b), and salinity (c) in Kaktovik Lagoon for entire deployment period from 17 August 2018 to 11 August 2019. The first section to the left of the dashed line is open phase 2018, the middle section is closed 2018 – 2019, and the last section to the right of the second dashed line is open phase 2019.

https://doi.org/10.5194/bg-2020-358
Preprint. Discussion started: 9 October 2020

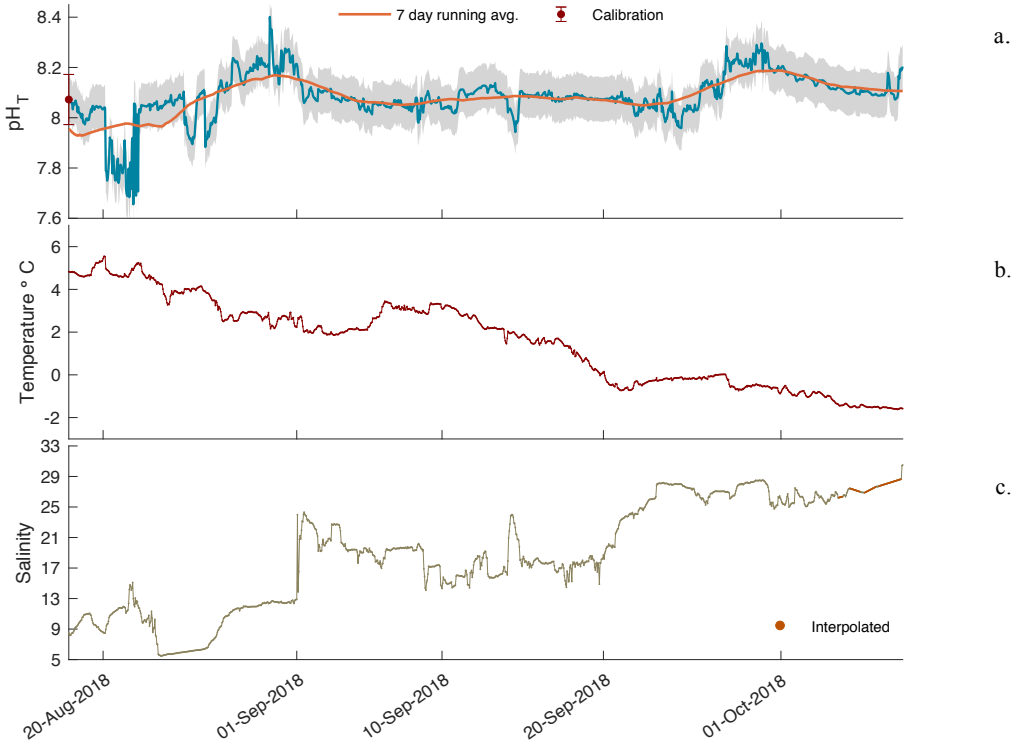

Figure 3. Open phase 2018 time series of pH_T (a), temperature (b), and salinity (c) in Kaktovik Lagoon.

https://doi.org/10.5194/bg-2020-358
Preprint. Discussion started: 9 October 2020

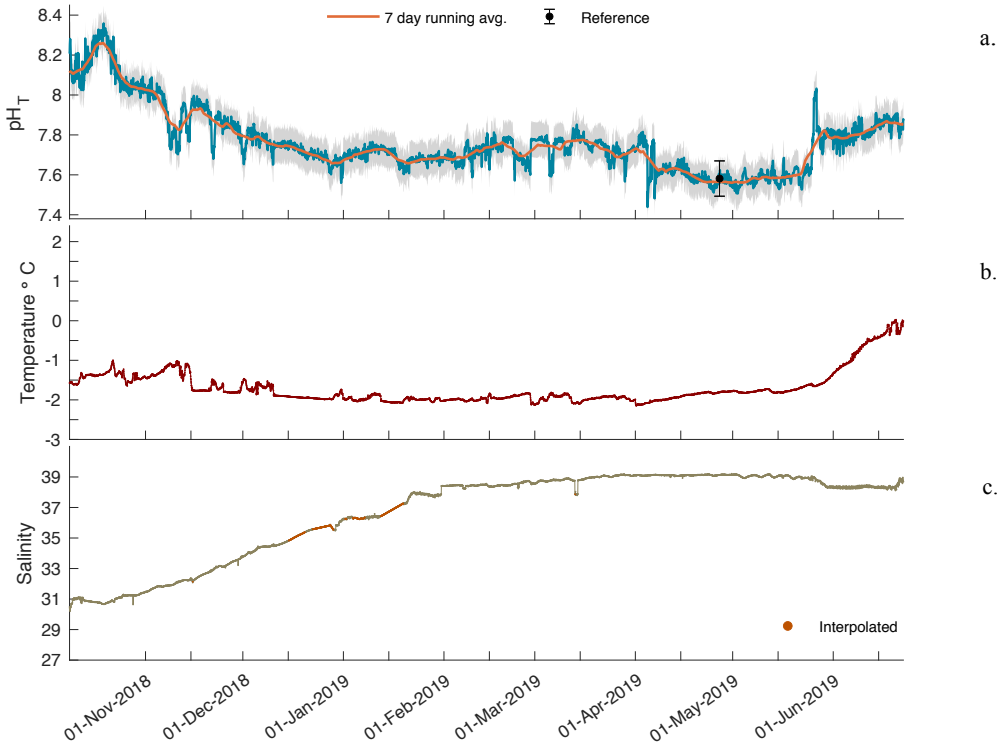

Figure 4. Iced phase 2018 – 2019 time series of pH$_T$ (a), temperature (b), and salinity (c) in Kaktovik Lagoon.

https://doi.org/10.5194/bg-2020-358
Preprint. Discussion started: 9 October 2020

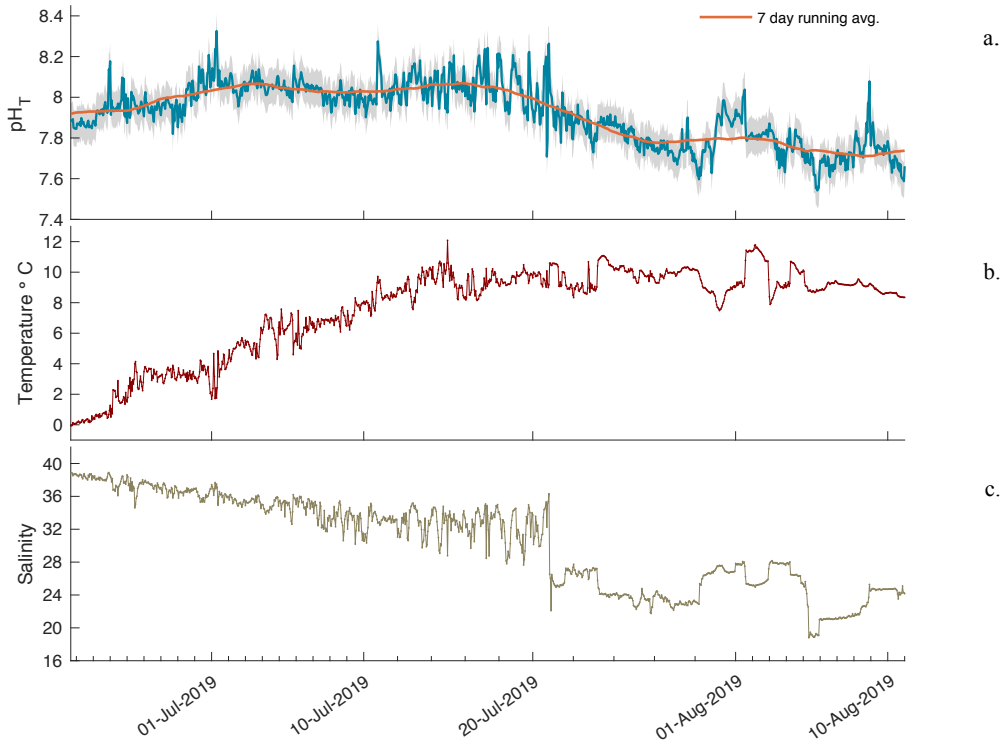

Figure 5. Open phase 2019 time series of pH_T (a), temperature (b), and salinity (c) in Kaktovik Lagoon.

https://doi.org/10.5194/bg-2020-358
Preprint. Discussion started: 9 October 2020

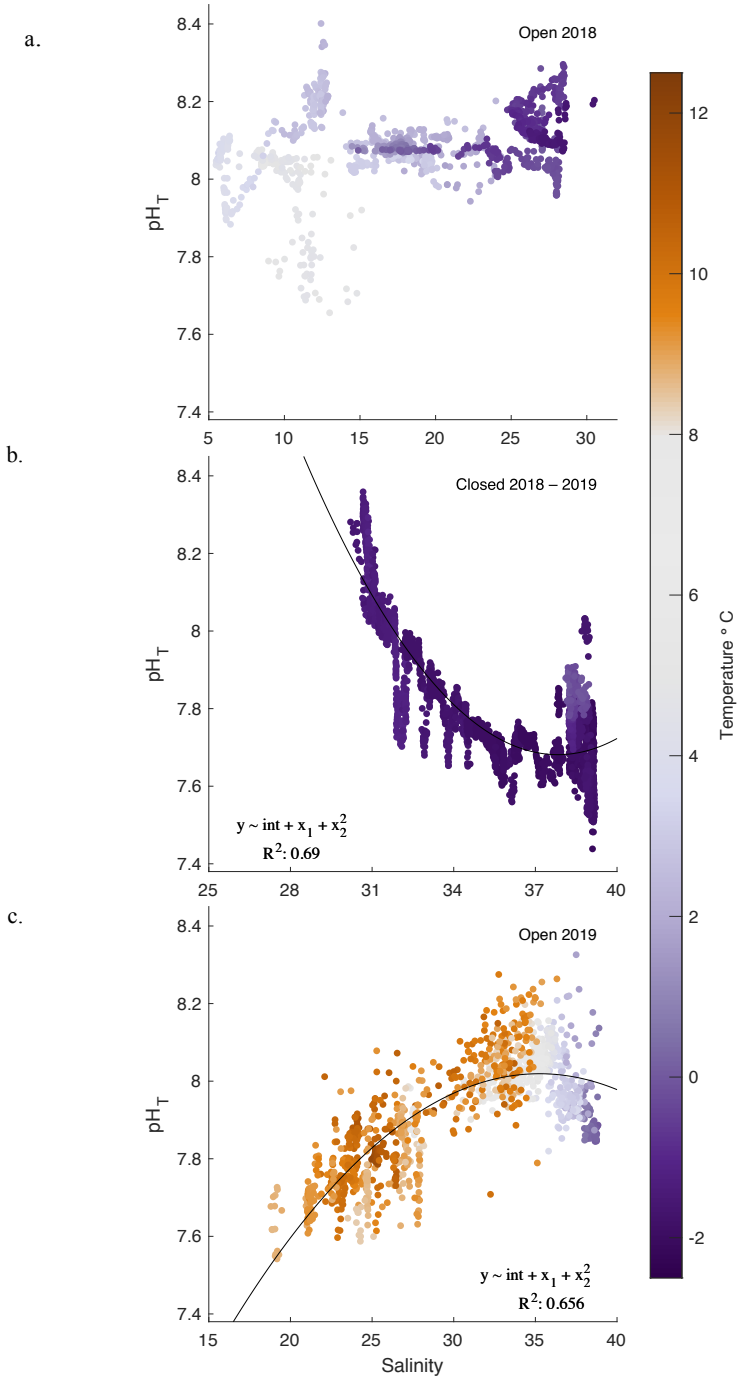

Figure 6. pH_T-salinity correlations for open 2018 (**a**), iced 2018 – 2019 (**b**), and open 2019 (**c**). Quadratic fits are applied to iced and open 2019 phases only. Temperature is represented in color for all correlations.

https://doi.org/10.5194/bg-2020-358
Preprint. Discussion started: 9 October 2020

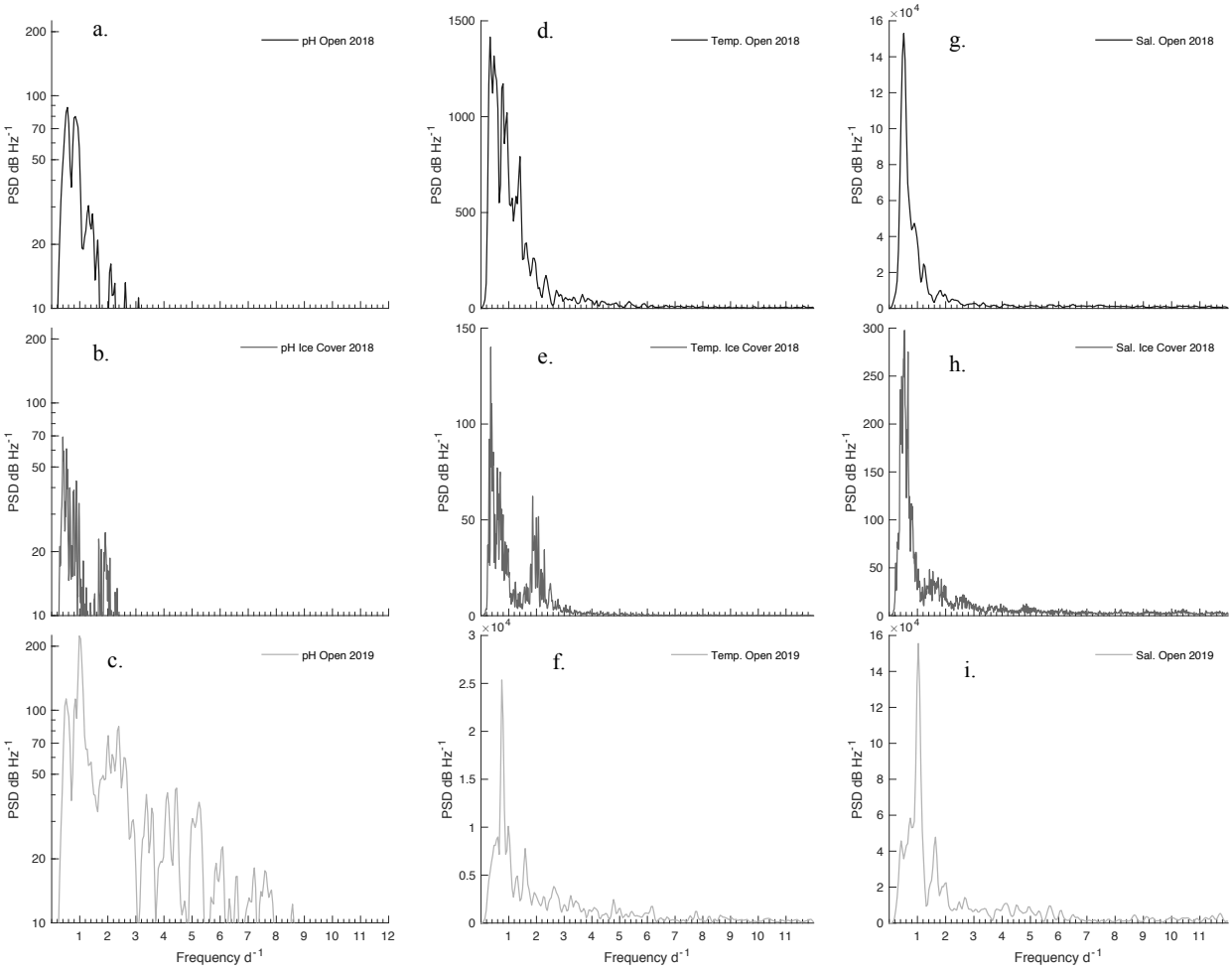

Figure 7. Power Spectral Density (PSD) plots for pH_T (a,b,c), temperature (d,e,f), and salinity (g,h,i) at each phase of the time series: open 2018 (top row), ice-cover 2018 – 2019 (middle row), and open 2019 (bottom row).

https://doi.org/10.5194/bg-2020-358
Preprint. Discussion started: 9 October 2020

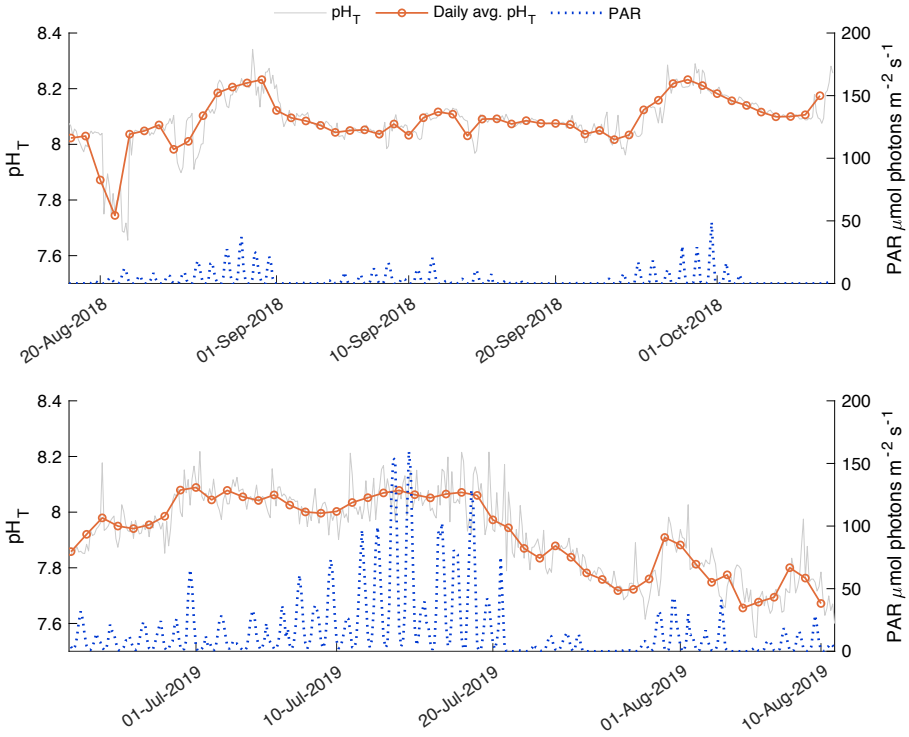

Figure 8. pH$_T$ (gray line) and PAR (blue dots) for open phase 2018 (**a**) and open phase 2019 (**b**). Daily average pH$_T$ (orange line) is displayed overtop hourly variability.

https://doi.org/10.5194/bg-2020-358
Preprint. Discussion started: 9 October 2020

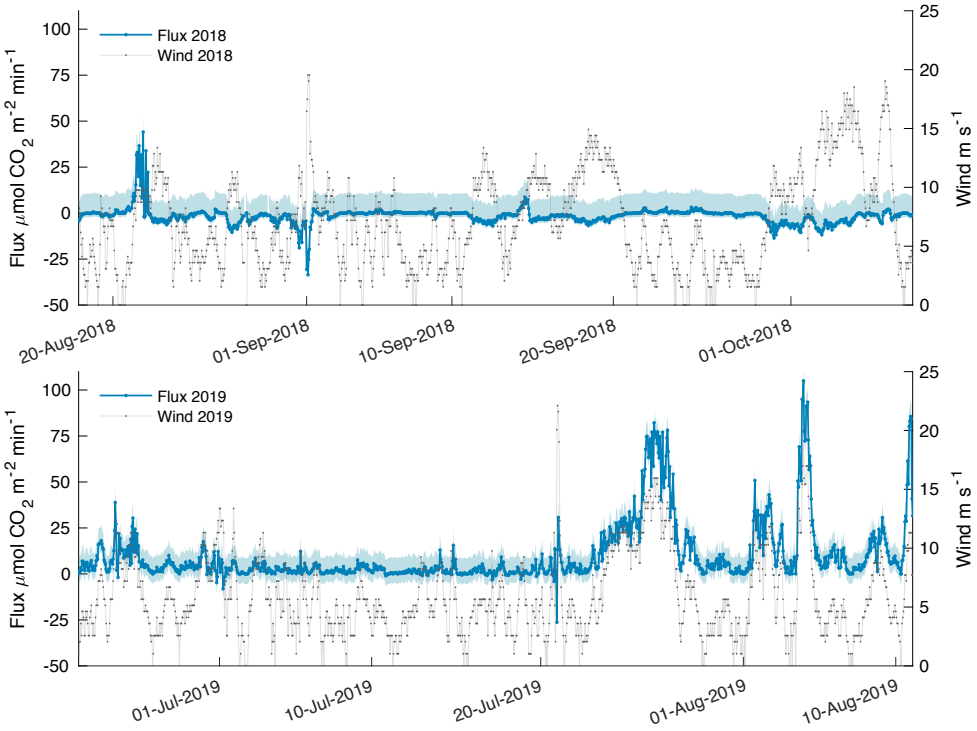

Figure 9. Estimated carbon flux (orange) and wind speed (grey) for open phase 2018 (**a**) and open phase 2019 (**b**). Uncertainty around each estimate is shaded in blue where the upper bound is associated with difference in PCO_2 from the A_T-salinity$_{in\ situ}$ regression, and the lower bound associated with freshwater Schimdt number. The upper and lower bounds for open 2018 were 10.67 and 2.23 μmol C m^{-2} min^{-1} while open 2019 upper and lower bounds were 8.56 and 5.52 μmol C m^{-2} min^{-1}, respectively.